NUMERICAL INVESTIGATION OF VORTEX FORMATION AT ASYMMETRIC HORIZONTAL INTAKES

A THESIS SUBMITTED TO
THE GRADUATE SCHOOL OF NATURAL AND APPLIED SCIENCES
OF
MIDDLE EAST TECHNICAL UNIVERSITY

BY

ALPER SUNGUR

IN PARTIAL FULFILLMENT OF THE REQUIREMENTS
FOR
THE DEGREE OF MASTER OF SCIENCE
IN
CIVIL ENGINEERING

AUGUST 2018

Approval of the thesis:

NUMERICAL INVESTIGATION OF VORTEX FORMATION AT ASYMMETRIC HORIZONTAL INTAKES

submitted by **ALPER SUNGUR** in partial fulfillment of the requirements for the degree of **Master of Science in Civil Engineering Department, Middle East Technical University** by,

Prof. Dr. Halil Kalıpçılar _____
Dean, Graduate School of **Natural and Applied Sciences**

Prof. Dr. İsmail Özgür Yaman _____
Head of Department, **Civil Engineering**

Prof. Dr. Mete Köken _____
Supervisor, **Civil Engineering Dept., METU**

Prof. Dr. Mustafa Göğüş _____
Co-Supervisor, **Civil Engineering Dept., METU**

Examining Committee Members:

Prof. Dr. Zafer Bozkuş _____
Civil Engineering Dept., METU

Prof. Dr. A. Mete Köken _____
Civil Engineering Dept., METU

Prof. Dr. A. Burcu Altan Sakarya _____
Civil Engineering Dept., METU

Assoc. Prof. Dr. Yakup Darama _____
Civil Engineering Dept., Atılım University

Asst. Prof. Dr. Önder Koçyiğit _____
Civil Engineering Dept., Gazi University

Date: 07.08.2018

I hereby declare that all information in this document has been obtained and presented in accordance with academic rules and ethical conduct. I also declare that, as required by these rules and conduct, I have fully cited and referenced all material and results that are not original to this work.

Name, Last name: Alper SUNGUR

Signature:

ABSTRACT

NUMERICAL INVESTIGATION OF VORTEX FORMATION AT ASYMMETRIC HORIZONTAL INTAKES

Sungur, Alper

M.S., Department of Civil Engineering

Supervisor: Prof. Dr. Mete Köken

Co-Supervisor: Prof. Dr. Mustafa Göğüş

August 2018, 82 pages

Given equations in literature for critical submergence depth is for symmetrical intakes; however, in practice, approach flow conditions are not symmetrical for most of the intakes. In this study, formation of the vortices in a horizontal water intake structure composed of a reservoir-pipe system is investigated with 3D numerical modelling using Flow-3D software. The geometrical and hydraulic conditions of the system such as the distance between the side walls of the horizontal intake, pipe diameters and the flow discharge are altered and the critical submergence depth required for the formation of the vortex for each case is determined and compared with the experimental results. It is observed that the critical submergence depths obtained from numerical simulations are very close to the experimental results. Hence, it can be concluded that Flow-3D is a reliable software to observe vortex formation at asymmetric horizontal intakes.

Keywords: Asymmetric horizontal intake, Air-entraining vortices, Vortex formation, Critical submergence, Flow-3D

ÖZ

ASİMETRİK YATAY SU ALMA YAPILARINDA VORTEKS OLUŞUMUNUN SAYISAL OLARAK İNCELENMESİ

Sungur, Alper
Yüksek Lisans, İnşaat Mühendisliği Bölümü
Tez Yöneticisi: Prof. Dr. Mete Köken
Ortak Tez Yöneticisi: Prof. Dr. Mustafa Göğüş
Ağustos 2018, 82 sayfa

Her ne kadar literatürde kritik batıklık derinliği için verilen denklemler simetrik su alma yapıları için verilmiş olsa da; pratikte su alma yapılarının çoğunda yaklaşım akım koşulları asimetriktir. Bu çalışmada, bir rezervuar-boru sisteminden oluşan asimetrik bir yatay su alma yapısında vortekslerin oluşumu üç boyutlu sayısal modelleme yöntemi ile Flow-3D yazılımı kullanılarak incelenmiştir. Su alma yapısı yan duvarları ara mesafesi, boru çapı ve akımın debisi gibi sistemin geometrik ve hidrolik şartları değiştirilerek, durumların her birisi için vortekslerin oluşacağı kritik batıklık derinliği tespit edilmiş ve deney sonuçları ile karşılaştırılmıştır. Üç boyutlu sayısal modellemelerin sonuçları ile deney sonuçları birbirine çok yakın bulunmuş olup; Flow-3D'nin, asimetrik yaklaşım koşullarına sahip yatay su alma yapılarında vorteks oluşumunu incelemek için güvenilir bir yazılım olduğu ortaya konulmuştur.

Anahtar Kelimeler: Yatay su alma yapısı, Hava girişli girdaplar, Vorteks oluşumu, Kritik batıklık derinliği, Flow-3D

To my dear son Deniz

ACKNOWLEDGEMENTS

I would like to give my special thanks to my supervisor Prof. Dr. Mete KÖKEN for his assistance, support and patience during my study.

I would like to thank to my co-supervisor Prof. Dr. Mustafa GÖĞÜŞ for his assistance throughout this study.

I would like to express my gratitude to my wife Sema SUNGUR, my mother Gülten SUNGUR and my grandmother Sevim KARATAŞ for their endless love, patience and confidence during my life.

I would like to thank Burak SUNGUR, Bilgin KARATAŞ, Yasemin KARATAŞ and Kübra KARATAŞ for their support and encouragement during my life.

I would like to express my appreciation to Ezgi KÖKER, Umut AYKAN, Emin Baturalp DOKEL, Muammer ŞİMŞEK, Sultan KILIVAN and Yücel YETGİN for their advices, helpfulness and friendship during my study period.

I would like to thank also Nursen TAMER, Mustafa TEKİN, Mustafa ULUCAN and Alperen TAMER from Pik Enerji Engineering and Construction Inc. for their patience and support during my study period.

The experimental results were taken from the study of Emre Haspolat which was supported by TUBITAK under Project No: 113M326.

TABLE OF CONTENTS

LIST OF TABLES

TABLES

LIST OF FIGURES

FIGURES

LIST OF SYMBOLS

b_{left}	Distance between the center of the intake and the left-side wall
b_{right}	Distance between the center of the intake and the right-side wall
D	Diameter of intake structure
Fr	Froude number of intake structure
h	Water depth at the reservoir of the intake
Δh_s	Water depth increment
Q	Inflow/Outflow discharge
S_c	Critical submergence depth measured from the summit point of intake pipe
S_c-exp	S_c measured in experimental study
t	Time
ω_z	Vorticity around z axis
z	Location of x-y plane on z axis
μ	Dynamic viscosity of the fluid
Γ	Circulation

CHAPTER 1

INTRODUCTION

1.1 Intake structures

Intake structures are used for collecting high quality water from the sources such as river, lake or dam reservoir. The usage of intake structures are listed below;

- Power production
- Drinking water supply
- Irrigation
- A trashrack to block debris
- Fish Passages
- Control gates and devices
- Diversion tunnels or conduits

There are no standard designs for intake structures. Each design is unique and may take many variations according to the project conditions such as geology, topology, hydrology and economic optimizations. However, some general design considerations may be followed such as;

a) The intake structure elevation must be over the sedimentation level of reservoir or lake.
b) The intake structure elevation must be lower than the minimum water surface elevation by critical submergence depth.
c) The geometry of the intake structure should be designed to minimize hydraulic loses.

Therefore, sedimentation and critical submergence depth are the most important requirements for intake design.

1.2 Definition of vortex

For low submergence conditions, vortices are formed at the reservoir of the intake structure. The coherent structure of rotational flow and circular streamlines is called a vortex.

According to the study of Durgin & Hecker (1978), three main reasons causes vortices (Fig 1.1);

a) Eccentricity of the approach flow
b) Velocity gradients
c) Obstruction

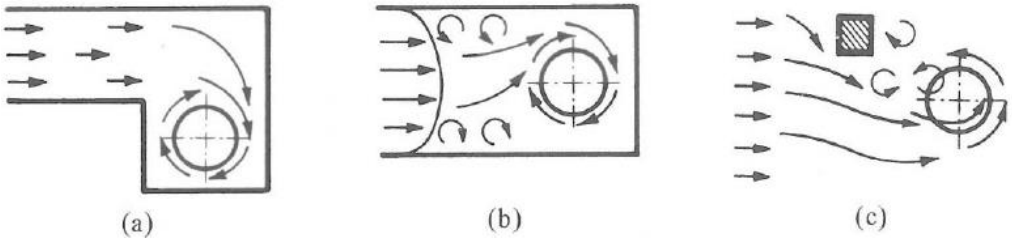

Figure 1.1 Sources of vorticity (Durgin & Hecker, 1978)

Vortices are classified visually according to the vortex strength intensity by Knauss (1987) which is given in Figure 1.2.

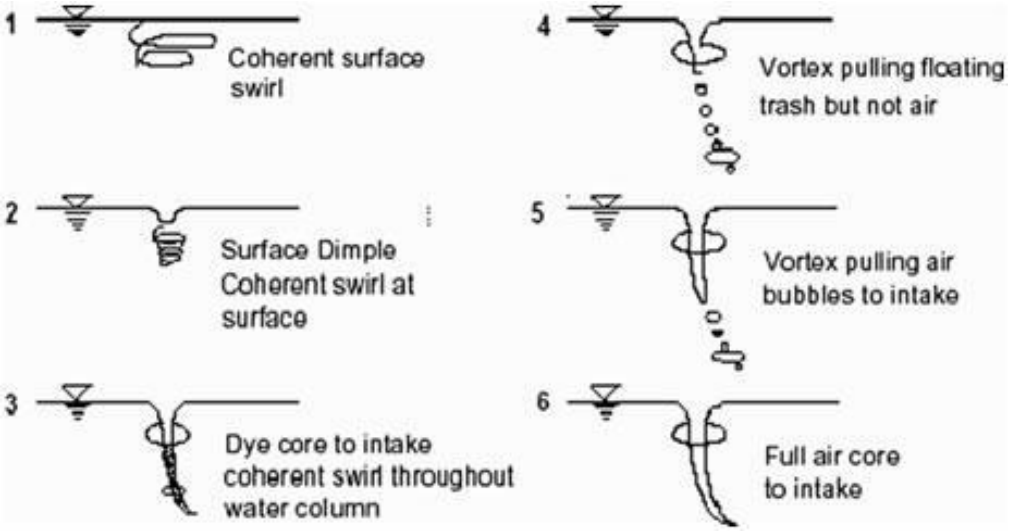

Figure 1.2 Classification of vortex types (Knauss, 1987)

1.3 Definition of critical submergence depth

For horizontal intakes, critical submergence depth is the vertical distance between intake and the free water surface just before the air-entraining vortex formation starts. The reference point of intake varies by researcher. The summit point of the mouth of intake structure or central axis of intake structure are the mostly used reference points in the literature. In practice each intake design is unique hence, there is not an exact mathematical expression to calculate critical submergence depth for different intake types in the literature.

1.4 Problems due to vortex

As mentioned above, intakes are designed according to the calculated critical submergence depth. In case the water depth on the intake is smaller than the critical submergence, undesirable situations arise such as;

- Cavitation oriented problems
- Vibrations which reduce the lifetime of machinery parts
- Entrainment of floating materials
- Increase of head loses and reduction of discharge capacity

1.5 Recommendations for prevention of vortices

For prevention of vortex formation; characteristics of approach flow should be modified, geometry should be improved or anti-vortex devices should be used.

Modification of approach flow can be done by;

- Geometrical changes for uniformity
- Approach channels that direct flow to intake
- Gate control
- Streamlining of piers and walls
- Acceleration of approach flow by changing geometry

Also, elongation of streamlines can prevent the vortices by;

- Lower intake elevation
- Increasing tail water submergence depth
- Horizontal structure at the top of intake
- Reducing the approach velocity with wider approach channel

Moreover, vertical rows of walls, horizontal beams, floating rafts and flow straighteners are used as anti-vortex devices.

1.6 Scope of the study

There is an experimental study for the determination of critical submergence depth of horizontal intakes conducted by Haspolat (2015). In his experiments, intakes with adjustable side walls in the approach channel are investigated to determine the critical submergence depth of the air entraining vortices.

In the present study, numerical model of the experimental setup of Haspolat (2015) is created to run 3D numerical simulations by computational fluid dynamics (CFD) software Flow-3D in order to assess the predictive capabilities of this code in terms of vortex formation. Critical submergence depths obtained from simulations are compared with experimental results, hence, the convenience of usage of Flow-3D software in determining the critical submergence depth for horizontal intakes is evaluated.

CHAPTER 2

LITERATURE REVIEW

Nowadays, computational fluid dynamics (CFD) has been widely used by researchers who investigate the vortex formation at the entrance of intake structures. On the other hand, experimental studies have been conducted to achieve valid empirical formulas for critical submergence depth of water intakes for decades.

Anwar (1968) conducted experiments and did theoretical research about vortex formation and the prevention of vortices for different flow types. He reached a conclusion that deep dimples and weak vortices are not related to radial Reynolds number which is higher than $1x10^3$.

Gordon (1970) investigated vortex formation at 29 servicing intakes of power plants and obtained empirical formulas for critical submergence depth as follows;

$$\frac{S_c}{D_i} = 1.70\ Fr \qquad 2.1$$

for symmetrical approach,

$$\frac{S_c}{D_i} = 2.27\ Fr \qquad 2.2$$

for asymmetrical approach flow conditions where Fr is the Froude number ($=V_i/\sqrt{gD_i}$), D_i is the diameter of the intake and S_c is the vertical critical submergence depth which is measured between free water surface and peak point of the intake structure.

Reddy and Pickford (1972) conducted flume experiments at horizontal intake structures to acquire valid formulas to calculate the critical submergence depth. Reynolds number and wave length were neglected since it was a free surface flow. As a result, two formulas were found as follows;

Setup without vortex prevention devices;

$$S_c/D_i=Fr \quad 2.3$$

Setup with vortex prevention devices installed;

$$S_c/D_i=1+Fr \quad 2.4$$

Knauss (1987) investigated the critical submergence depth of intake structures of hydroelectric power plants and stated the minimum reservoir conditions to avoid vortices as shown in Figure 2.1.

Yıldırım and Kocabaş (1995) studied on the critical submergence depth of intakes experimentally. Rankine's half body which consists of uniform channel flow and a point sink, was used to measure the critical submergence depth of a vertical intake. At the end of the study, a dimensionless formula was derived to decide on the critical submergence depth.

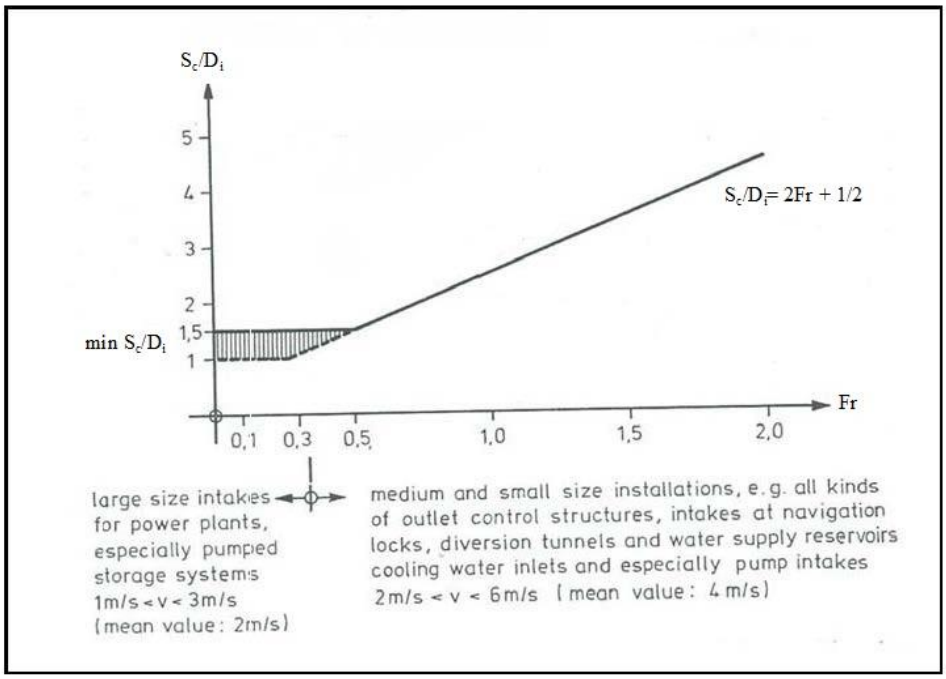

Figure 2.1 Recommended submergence depth for intakes (Knauss, 1987)

Haspolat (2015) conducted experiments to investigate the formation of air entraining vortices under symmetrical and asymmetrical approach flow conditions at horizontal intakes. Four horizontal intake pipes with different diameters were used. In addition, adjustable side walls were placed to create symmetrical and asymmetrical approach flow conditions. A dimensionless equation for the critical submergence was derived as a function of related geometric and hydraulic parameters. By using regression analysis, empirical equations were derived to determine the critical submergence depth and compared with the similar ones in the literature.

Göğüş, Köken and Baykara (2016) investigated the effects of hydraulic parameters on the formation of air-entraining vortices at horizontal intakes without approach flow induced circulation. Six different diameters were used as horizontal intake pipe in the study. The reservoir setup had adjustable channel sidewalls. Experiments were conducted to find critical submergence depths with different discharge values and sidewall clearances. Empirical

equations were derived for the dimensionless critical submergence as a function of the relevant dimensionless parameters. These obtained equations showed a quite good agreement with the similar ones in the literature.

Gürbüzdal (2009), Sarkardeh et. al (2010), Taştan and Yıldırım (2010) also investigated the vortex formation experimentally.

Numerical studies have been also conducted to investigate vortex formation and decide critical submergence depth of water at intake structures.

Rosenhead (1931) made an approximation to a vortex sheet by changing the continuous distribution of vorticity with appropriate discrete point vortices. During the investigation of the effects of a general disturbance, singular wave-length was used instead of all wave lengths. 2, 4, 8, 12 vortices to a wave-length were used for numerical calculations. However, Moore (1971) and Takami (1964) conducted experiments which indicated that point vortex method is unstable.

Chorin (1973) introduced the 3D vortex blob calculation which is a vortex filament method. He used vorticity blobs instead of point vortices to solve time dependent Navier-Stokes equations for high Reynolds numbers. In this method, point vortex was selected as the center of circle containing the velocity field. This study was a milestone of numerical vorticity calculation.

Hald and Del Prete (1978) presented the two-dimensional proof of Chorin (1973)'s vortex blob method for inviscid flow of incompressible fluid. Proof showed that a solution exists for short times, provided that, the vortex blobs overlaid to each other. Hald (1979) proved second-order convergence for long time period.

Beale and Majda (1982a, 1982b) formulated a different type of 3D vortex methods and proved that these new methods have high order accuracy and stability. In addition, the computational time of these vortex algorithms of Lagrangian stretching are approximately same as Chorin (1973)'s algorithms.

Nagahara et al. (2003) conducted an experiment to measure the flow around vortex formation of a pump intake and they compared the velocity fields of experimental setup with CFD calculations. Particle image velocimetry (PIV) was used to observe the velocity fields of experimental setup. Circulation values of both CFD and PIV were approximately same, on the other hand, maximum velocity values of CFD calculations were smaller than the experimental values. Moreover, the instant maximum velocity values were larger than time-averaged values and vortex core radii were smaller because of the unsteadiness of vortex formation. As a result, the accuracy of CFD calculations was not reliable even if the grid distribution was sufficient.

Okamura et al. (2007) ran numerical simulations of pump sumps with different CFD codes. Results of this study are listed below;

- The critical submergence depths of submerged vortex and air entrained vortex were roughly proportional to the rate of flow.
- CFD codes were reliable for prediction of vortex formation and its location visually.
- Even if velocity distribution at intake mouth agreed with the experiments, vorticity strength and distribution pattern of the vorticity were different.
- The critical submergence depth was not decided by visible vortex formation. An extra process (vortex core static pressure) was needed to decide the critical submergence depth.

Li et al. (2008) conducted experiments to investigate the free surface vortex formation and also compared the experimental results and numerical simulations. Dye was used to follow the streamlines of vortex structure. In addition, the flow fields of different stages were measured with PIV. As a result; they concluded that the position of vortex and the structure of vortex core were same for both experimental and numerical models.

Nakayama and Hisasue (2010) made a 3D numerical simulation of the intake reservoir of a small-scale hydropower facility. Large eddy simulation (LES) solver was used to simulate the 3D unsteady flow of this power system. The features of unsteady flow, the formation of vortices, surface profiles were simulated well compared with the experimental model. Even if long time simulation and experimental results had some differences, simulation results were reliable.

Chen et al. (2012) compared volume of fluid method with different turbulence models to find the best simulation method for vertical vortex formations. Viscosity, dissipation rate and kinetic energy values of turbulent flow and their effects on vertical vortex formation were investigated. Simulation results indicated that RNG k - ε model was more suitable than k - ε model to simulate vertical vortices due to the curved and immediately strained streamlines.

Zhao and Nohmi (2012) investigated the accuracy of volume of fluid method for free surface flows of pump intakes. Two cases were introduced at this study. In the first case, large eddy simulation (LES) method was used to measure the circular velocities around the vortex formation instead of Reynolds averaged Navier-Stokes (RANS) turbulence model. The results of numerical simulation were compared with the experimental results of Turbomachinery Society of Japan. In the second case, flow rate distribution of pump structure was investigated. The pump system had two closed and one open channels. The analysis results of VOF method were compared with fixed water surface method (FWSM). It was concluded that VOF technique was reliable to decide visible vortex for industrial use. Moreover, in the second case VOF method did not agree with FWSM method because of boundary condition options at water-air interface.

Sarkardeh et al. (2014) compared numerical and experimental results of flow movement in a reservoir in terms of vorticity. The intake had a constant submergence and 2 different Froude numbers. Acoustic Doppler Velocimeter

(ADV) was used to measure the velocity fields. It was concluded that numerical simulation results agreed well with vorticity theories. Also, numerical and experimental results were close to each other. Only there was a difference in maximum velocity about 10%. A funnel shape flow was observed at the entrance of the intake. It was recommended that additional studies with finer grid resolution were needed for better understanding of flow movement.

Tataroğlu (2014) investigated the formation of vortices in an intake structure composed of a pipe-reservoir pumped flow system by using Flow-3D. Experimental studies of Baykara (2013) were numerically modelled and the critical submergence depths are found. The results of experimental and numerical studies were compared with each other. According to the comparison, Large Eddy Simulation (LES) results are found to be closer to the experimental results compared to the laminar solutions. It is stated that laminar solver was not able to capture the vorticity near walls that is resulting from turbulence. She also studied the effect of anti-vortex plate and model scale effect.

CHAPTER 3

NUMERICAL MODELLING

3.1 Introduction

Flow-3D is a software for computational fluid dynamics (CFD), developed by Flow Science, Inc. This software uses Volume of Fluid (VOF) method to solve problems that involve free surface flows. Moreover, moving and deforming solids, heat transfer, surface tension and phase change models are available for other engineering analyses.

Volume of Fluid (VOF) method is used to solve free surface flow problems by tracking and locating the free surface or fluid-fluid interface. Even if VOF method is known before, the first publication in a journal was by Hirt & Nichols in 1981. The use of this method become more popular with the increase in computational power.

Even though there are various CFD software, Flow-3D is used in this study. One reason is that it is more powerful in simulation of the free surface flows as it uses an improved VOF algorithm called TruVOF in solving the free surface. Another reason is that Flow-3D uses a non-body-fitted gridding technique which makes meshing process simpler and easier compared to the other CFD codes that use body fitted meshes.

3.2 Model setup

Flow-3D has a very friendly user interface. Model setup menu has six submenus which are general, physics, fluids, meshing & geometry, output and

numeric tabs. If this order of submenu items is followed, it is easier to model any flow problem.

In the general submenu, simulation finish time, interface tracking method, flow mode, number of fluids, unit and version options are decided. Simulation finish time is set to 50 seconds for all cases. Interface tracking method is selected as free surface or sharp interface. Moreover, flow is assumed incompressible and a single-phase solution is made. SI units are used for all the simulations. The version option is chosen as double precision for a higher precision.

Gravity components, wall shear boundary conditions, viscosity and turbulence options are defined under the physics submenu. Gravity z component is defined as -9.81 m/s^2 so gravity acts in negative z-direction. Wall shear boundary is selected as no slip or partial slip. Viscous flow is used for all cases and Large Eddy Simulation (LES) is selected for turbulence option.

In the fluid submenu, fluid properties are defined.

The next part is the meshing & geometry submenu. First, different components are modeled by using geometric shapes and properties are assigned to these shapes according to their purposes (Figure 3.1). A rectangular solid component is created to represent the intake structure which has also a cylindrical hole component to form the outflow pipe. Another rectangular solid prism is used for bottom of channel. Further, a spherical solid component is selected to perform as a mass source which represents the inflow pipe in the physical model. Flow rate type of mass source is selected as “volume flow rate” and the discharge is defined as a function of time as given in Figure 3.2. Discharge is gradually increased up to the designed discharge in 5 seconds, in order to prevent a wave formation in the reservoir.

Finally, two solid components are placed as impervious walls over mass source for preventing the possible fluctuations in the reservoir free surface. The components of the numerical model are shown below in the Figure 3.1.

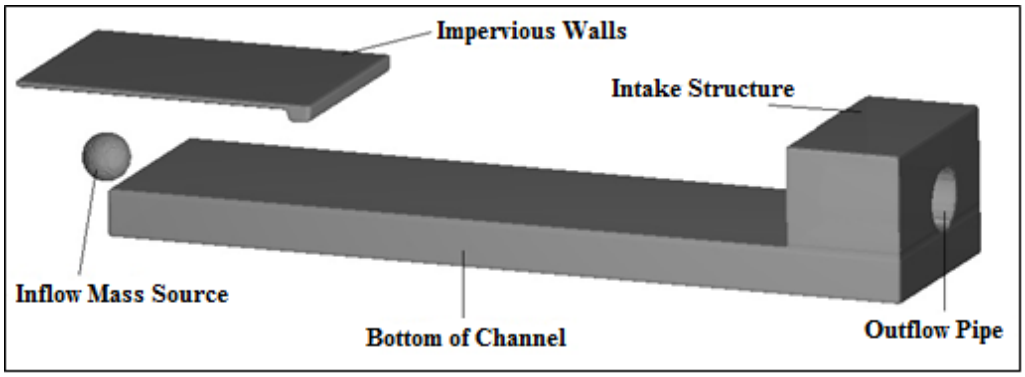

Figure 3.1 Components of the numerical model

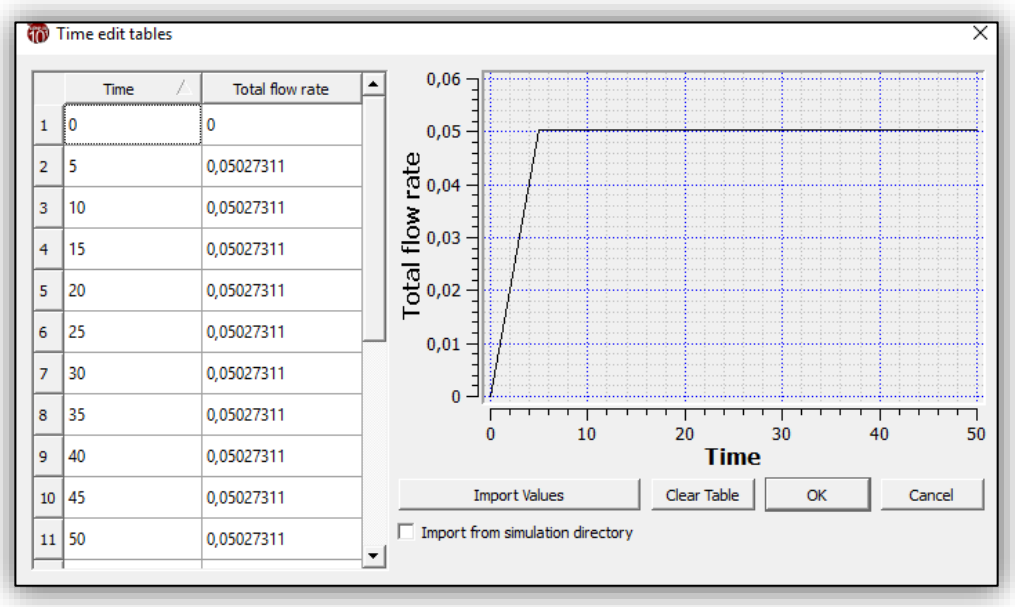

Figure 3.2 An example table of mass source flow rate

In the numerical models, flow and geometrical characteristics for each case are set according to the experimental cases of Haspolat (2015). The diameter of outflow pipe (D) and distance to the side walls of reservoir (b_{left}, b_{right}) are defined. Since the critical submergence depths for different asymmetrical cases are the subject of this study, the reservoir water depth is the only variable left to be set for each case. First, the reservoir water depth (h) of the experimental case where vortex formation was observed, is set as the reservoir water depth in the numerical model. Then, by increasing/decreasing the water depth and rerunning the simulation, the critical submergence depth (S_c) is decided. For all cases, 2.50 cm step size is used as a water depth increment except the prototype cases. The initial geometric parameters used in the simulations are shown below in Figure 3.3.

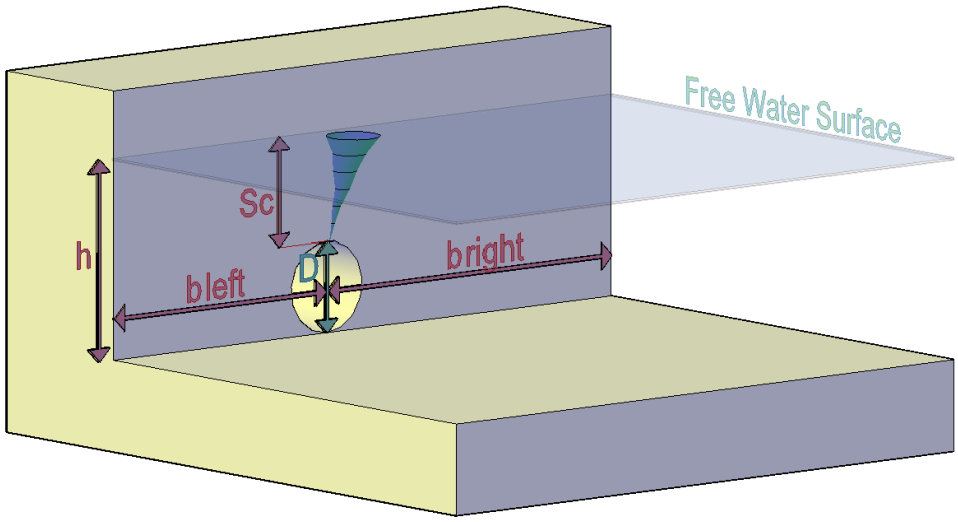

Figure 3.3 A sketch of a horizontal intake structure with geometric parameters

After the completion of the model geometry, grid generation and boundary conditions are decided under the meshing&geometry submenu. Flow-3D uses non-body-fitted gridding technique which separates meshing from geometry construction. By that, grid or geometry can be freely changed without affecting each other due to the independency between grid and geometry. Rectangular and cartesian mesh system is used.

The size of the reservoir must be chosen by an optimization between computational time versus accuracy. The mesh volume must be large enough to ensure the accuracy of numerical model, however the larger mesh volume increases the computational time which is not economically feasible.

In these cases, the length of the mesh block is fixed as 3.40 m for cases with 25 cm pipe diameter and 2.40 m for cases with 10 cm pipe diameter, on the other hand, the width and the height of the mesh block covary with side wall clearance and reservoir water depth. The height of the mesh block is selected a little bit higher than the reservoir water depth due to the possible fluctuations of the water surface.

As mentioned earlier, grid size selection is crucial for computational time and accuracy of the numerical model. In the first trial one whole mesh block with 0.015 m grid size is selected. For different reservoir water depth values, vortex formation is not observed. It means grid size must be decreased, but an increase in the mesh size of whole block will cause unfeasible computational time. Hence, a second finer mesh block which has 0.003 m grid size is created just close to the intake mouth where possible vortex formation is expected to occur. By that, vortex region is analyzed with a finer mesh without increasing the total mesh number a lot. The grid of the mesh setup is shown in Figure 3.4.

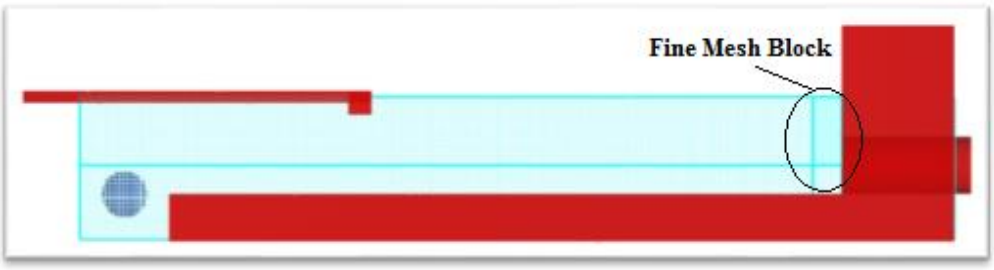

Figure 3.4 Solid components and mesh blocks

Finally, the boundary conditions must be defined for each face of the rectangular mesh blocks. Each face of the fine mesh block which is located at the vortex region is described as grid overlay (G). By that, the fine mesh block becomes embedded into the outer coarse mesh block. The side faces, bottom and the upstream face of the coarse mesh block are set as walls (W), which behaves as a solid structure with no-slip boundary condition. Top face of coarse mesh block is selected as symmetry (S). Hence, there is no flow through these faces and velocity is zero perpendicular to the faces. For downstream face, boundary is chosen as volume flow rate denoted by Q. Discharge rate is defined the same as the inflow mass source, and intended reservoir conditions are provided by that. Figure 3.5 shows the boundaries of the mesh blocks.

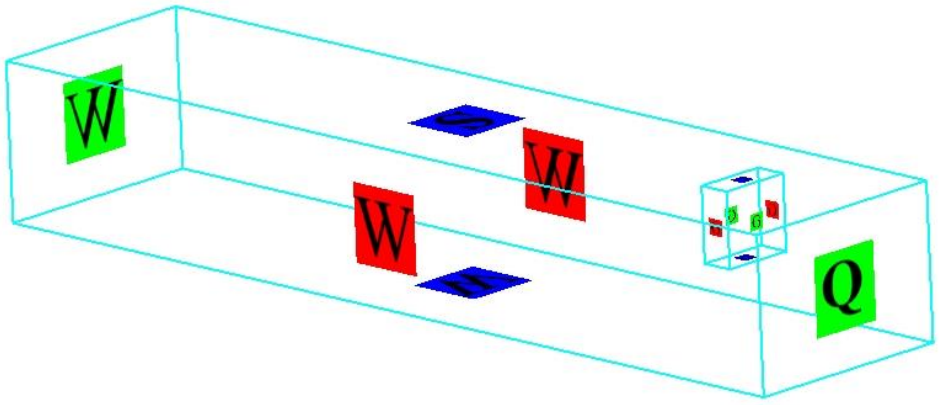

Figure 3.5 Boundaries of the mesh blocks

3.3 Simulation procedure

18 different experimental cases of Haspolat (2015) are studied in this thesis. Also, one of the cases is selected and simulated for grid size dependency check. Moreover, simulations in prototype scale are made. As a result, totally 20 numerical models are analyzed within this study.

First, each case is simulated with the same initial depth of matchup experimental case. After completion of initial case, the results are observed for vortex formation with a CFD post-processing tool. If a vortex formation is observed at first trial, a higher reservoir water depth is selected and another simulation is run until a case without vortex formation is observed. On the contrary, if a vortex formation is not observed at first trial, then a lower reservoir water depth value is used and a new simulation is run until a vortex formation is observed. In changing the water depth 2.50 cm increments (Δh_s) are used. By this procedure, the critical submergence depth is decided. The simulation procedure is summarized in Figure 3.6.

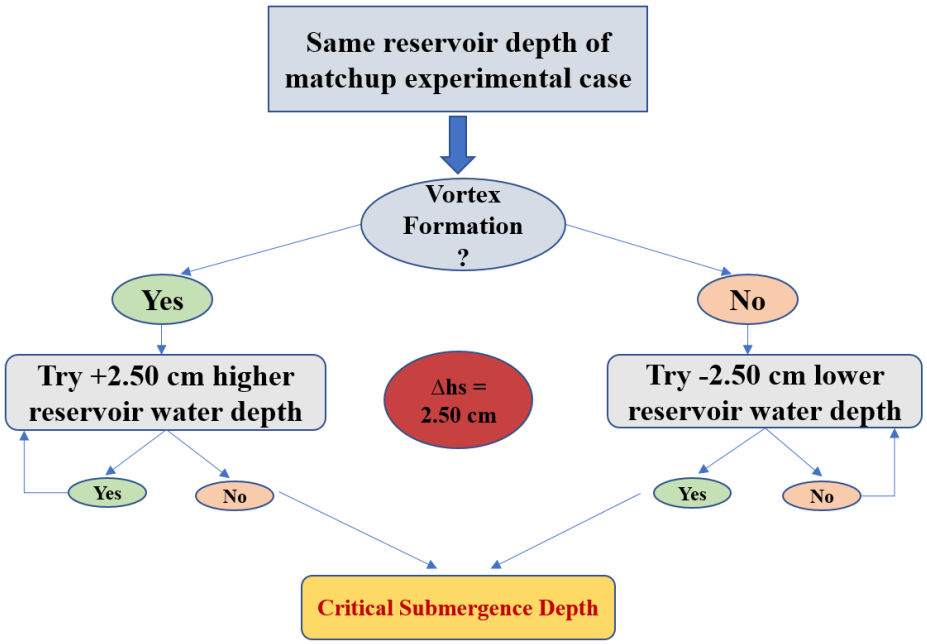

Figure 3.6 Simulation procedure

Computational time of these trial and errors is the key factor for applicability. To decide the critical submergence depth (S_c) of one case, approximately 5~6 runs are needed. Since, computational time of one simulation is about 24 hours in a workstation whose properties are listed in Table 3.1; the time consumed on each case is about one week including runs and analyzes if there are no other software related problems. In addition, computational run time of prototype case takes about 10 days with the workstation mentioned above. In conclusion, total computational time of whole study is about 4,560 hours which is 190 days.

Table 3.1 Computer specifications

Model:	Dell Precision T7600 Tower Workstation
Processors:	2x Intel® Xeon™ E5-2650 2.00GHz Eight (8) Core 20MB
Memory:	128GB (16x 8GB) PC3-12800R Memory
Raid Controller:	Dell Perc H310 Raid Controller
Graphics Card:	Dell Nvidia Quadro 4000 2GB Graphic Card
Software:	Windows 10 Pro 64-bit

All the simulations run with their related parameters are listed below in Table 3.2.

Table 3.2 Study cases and properties

	Case Parameters				Grid Size		Physical Experiment
Case No	D (cm)	b_{left} (cm)	b_{right} (cm)	Q (l/s)	Coarse	Fine	S_c-exp (cm)
1	25.00	20.00	60.00	45.03	573,420	497,250	14.10
2	25.00	20.00	70.00	41.66	608,400	508,950	11.60
3	25.00	30.00	50.00	46.75	606,320	540,000	18.60
4	25.00	30.00	60.00	46.75	686,400	464,400	19.10
5	25.00	30.00	70.00	46.75	731,640	399,900	17.90
6*	25.00	40.00	50.00	50.27	655,200	430,000	17.60
7*	25.00	40.00	50.00	50.27	484,272	322,959	17.60
8	25.00	40.00	60.00	51.17	766,480	540,000	20.60
9	25.00	40.00	70.00	52.98	835,120	540,000	26.90
10	25.00	50.00	60.00	46.75	797,160	500,000	18.90
11	25.00	50.00	70.00	44.18	915,200	540,000	19.70
12	25.00	60.00	70.00	49.38	995,280	540,000	21.40
13**	10.00	20.00	30.00	16.64	257,400	485,550	15.10
14	10.00	20.00	40.00	17.23	312,000	485,550	14.70
15	10.00	20.00	50.00	16.64	253,988	348,300	13.20
16	10.00	30.00	40.00	17.84	272,130	332,000	23.90
17	10.00	30.00	50.00	22.92	358,015	432,000	22.30
18	10.00	40.00	50.00	22.92	316,800	400,000	25.20
19	10.00	50.00	60.00	28.47	521,293	258,687	25.80
20**	100.00	200.00	300.00	5260.00	2,231,376	3,537,800	Prototype of Case 13

* Grid dependency check of same case with different grid size
** Case 20 is the prototype of Case 13

3.4 Viscous solver

Flow type is defined as viscous with no-slip condition on the walls. Momentum equations are solved as second order in order to capture the swirling flows.

Tataroğlu (2014) studied vortex formation at horizontal intakes and compared Reynolds Averaged Navier-Stokes (RANS) model and Large Eddy Simulation (LES) turbulence model with the experimental results. Flow-3D was used for the simulations same as this study. It was stated that the results of LES turbulence model were more accurate and closer to the experimental results compared to the RANS model results. In addition, Tataroğlu implied that LES turbulence model is more suitable for capturing the vorticity near the walls.

Hence, LES turbulence model is used within the current study for all the cases. This model is based on Kolmogorov's (1941) similarity theory of turbulence which treats large scales and small scales individually. Large eddies of the flow are explicitly resolved, on the other hand, the impact of small eddies is parametrized by using sub grid-scale model (SGS). By that, the effects of unresolved small-scale fluid motions are taken into account implicitly.

3.5 Grid Size Dependency

Grid size optimization is the key of inexpensive simulation and accuracy. To observe grid size dependency different mesh sizes are used for the same model of a selected test case. Two simulations are run where one of the simulations is 25% coarser than the other one. The computational time, circulation values and vortex visualizations are compared to each other and the mesh size is decided for the rest of the cases.

The selected test case has a 25.00 cm outflow pipe and 50.27 l/s discharge value. Side clearances are 40 cm to the left side and 50 cm to the right side. The results obtained with a finer and a coarser mesh are given below in Table 3.3.

Table 3.3 Grid dependency results

Case No	Run Time	Grid Size		Numerical Results		Observation time
	(hour:min)	Coarse	Fine	S_c (cm)	Γ (circulation)	t (sec)
6	23:45	655,200	430,000	15.000	-2.70E-02	27.80
7	18:21	484,272	322,959	15.000	-2.61E-02	42.00

As seen the critical submergence depth does not change in both cases. Also, circulation values which are obtained on a horizontal plane just above the top of the intake pipe are roughly the same, only 3.33% difference occurs. That means fine mesh and coarse mesh cases agree with each other in terms of vorticity and critical submergence. Vorticity contours on a horizontal plane just above the top of the intake pipe are shown in Figures 3.7 and 3.8.

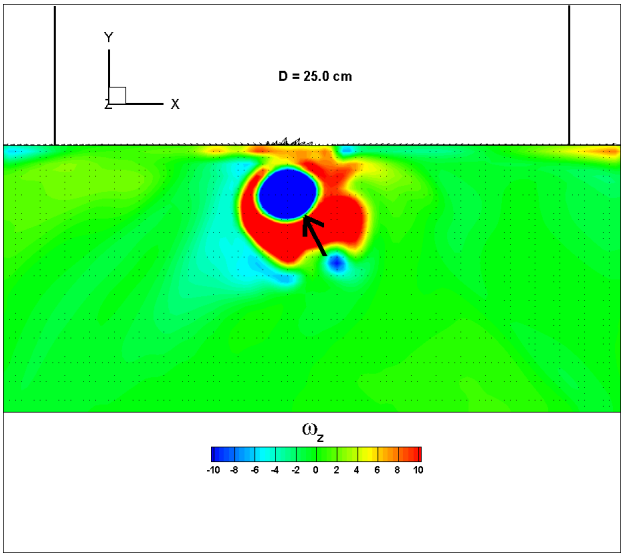

Figure 3.7 Case 6 (fine mesh): Horizontal vorticity contours (ωz, 1/sec) at the level of the just above top point of the intake pipe, z = 28.00 cm

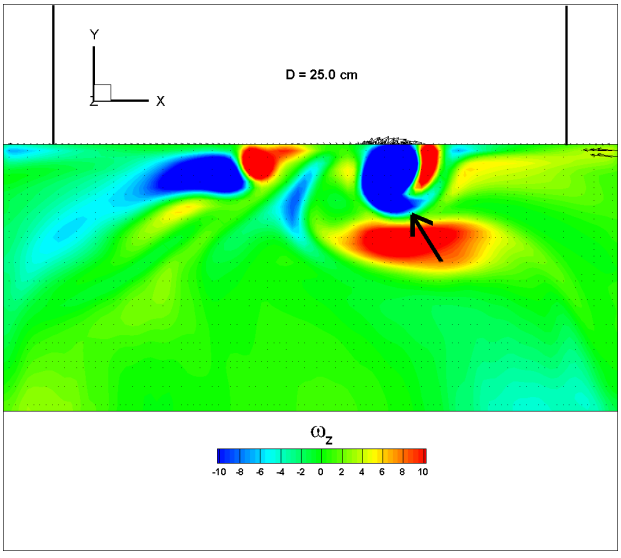

Figure 3.8 Case 7 (coarse mesh): Horizontal vorticity contours (ωz, 1/sec) at the level of the just above top point of the intake pipe, z = 28.00 cm

On the other hand, compared with the finer mesh, in the coarser mesh the visible full air core vortex depth decreases 56% from 3.14 cm to 1.40 cm due to the coarser mesh structure as seen in Figure 3.9 and Figure 3.10.

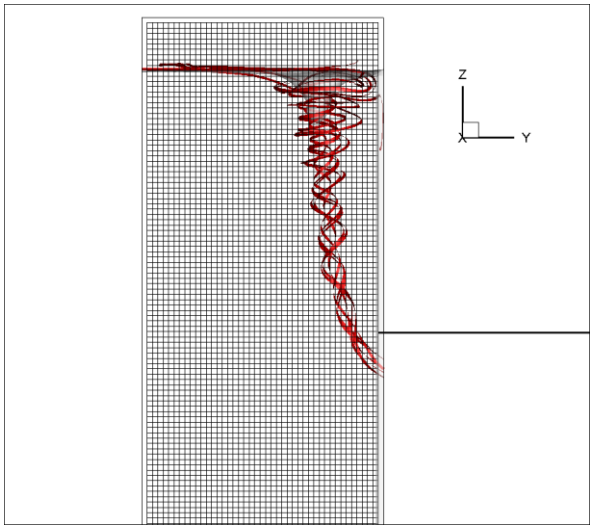

Figure 3.9 Air-water interface isosurfaces together with the 3D streamlines for fine mesh at t = 27.80 sec

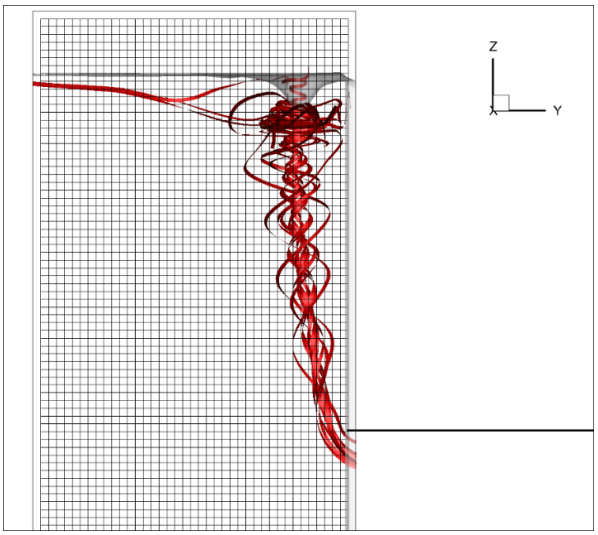

Figure 3.10 Air-water interface isosurfaces together with the 3D streamlines for coarse mesh at t = 42.00 sec

Since the computational time difference is not dramatically huge, the finer mesh option is selected for the rest of the simulations. That finer mesh option has 0.015 m coarse and 0.003 m fine grid size as mentioned at Model Setup section.

CHAPTER 4

RESULTS OF ANALYSES

4.1 Introduction

In this chapter, effects of discharge, sidewall clearance and scale are discussed. The experimental results and numerical results are compared to each other for accuracy. All the analysis results including vorticity and streamline cross sections from different regions are shown at Appendix A.

While determining the critical submergence depth in numerical simulations, water depth is changed with the increments of 2.50 cm (Δh_s). Which means there could be another vortex formation between the found critical submergence depth and somewhere within 2.50 cm higher depth. In other words, the error range is +2.49 cm for these numerical experiments.

The vortex region which is close to the water surface is easy to observe but when you get further away from the water surface towards the intake pipe, it is hard to see an air-core formation, because the vortex core is getting smaller and thinner. In this case, finer mesh option can be helpful in visualizing a larger portion of the air-core however, using a finer mesh size means an inapplicable expensive solution. At this point, circulation values and vorticity contours become important parameters in deciding whether it is a full air core vortex to the intake or not.

4.2 Effect of Discharge

In this study, an exact correlation is not found between discharge and critical submergence depth. But there is a trend which higher discharge value means higher critical submergence depth as seen in Figure 4.1 and Figure 4.2. Since, the sidewall clearance, variable for all cases, is also a governing parameter for critical submergence depth, an accurate comparison is not exactly possible.

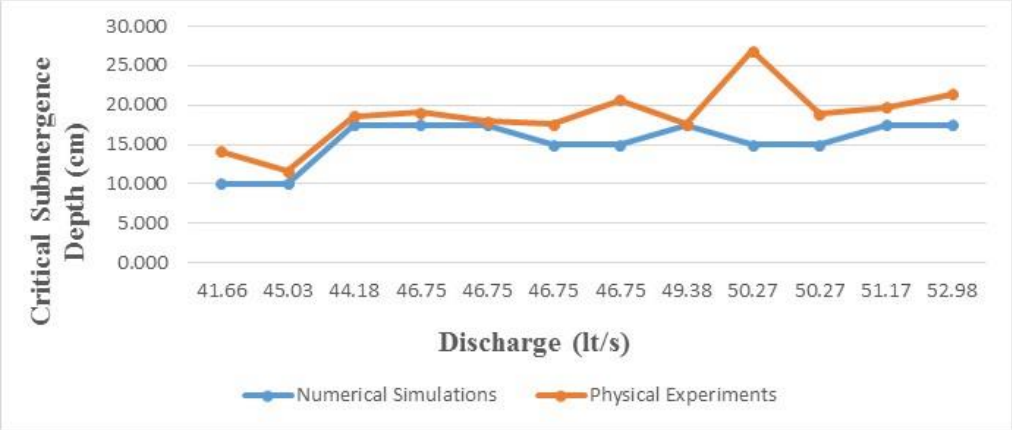

Figure 4.1 Discharge (l/s) vs Critical Submergence Depth (cm) Graph for intake pipe with 25.00 cm diameter

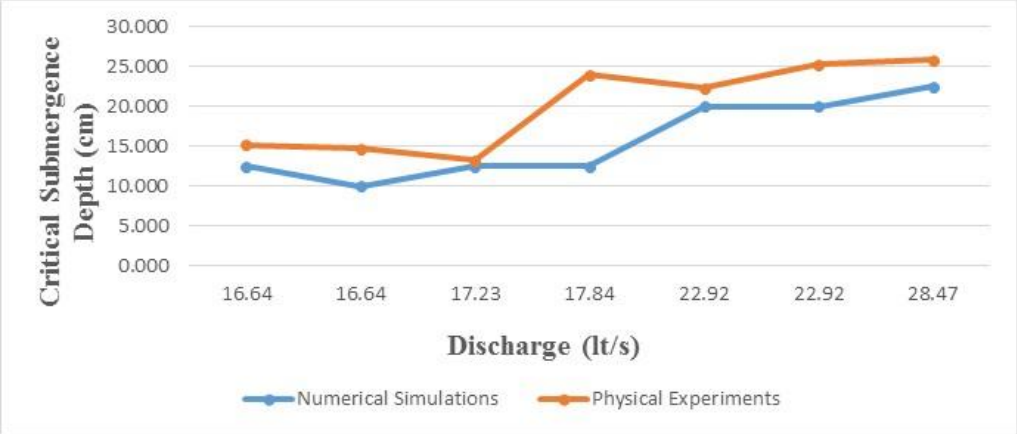

Figure 4.2 Discharge (l/s) vs Critical Submergence Depth (cm) Graph for intake pipe with 10.00 cm diameter

Gravity flow is used instead of pumped flow in the experimental setup of Haspolat (2015) and correspondingly in this numerical study. The plan and side views of experimental setup without a pump are shown in Figure 4.3 and Figure 4.4. On the other hand, in the similar numerical study of Tataroğlu (2014) and experimental setup of Baykara (2013), flow is pumped out of the reservoir as shown in Figure 4.5 and Figure 4.6 which is therefore defined as a pumped flow.

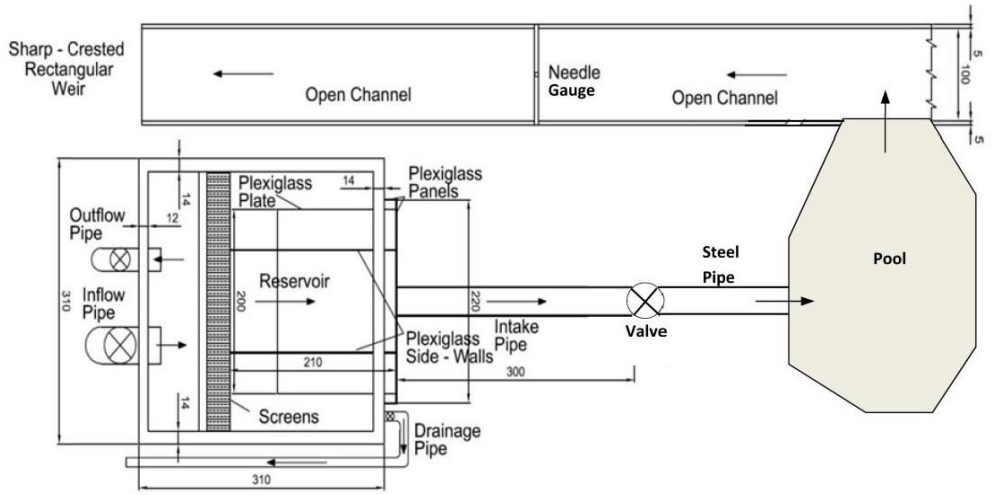

Figure 4.3 Plan view of experimental setup of Haspolat (2015)

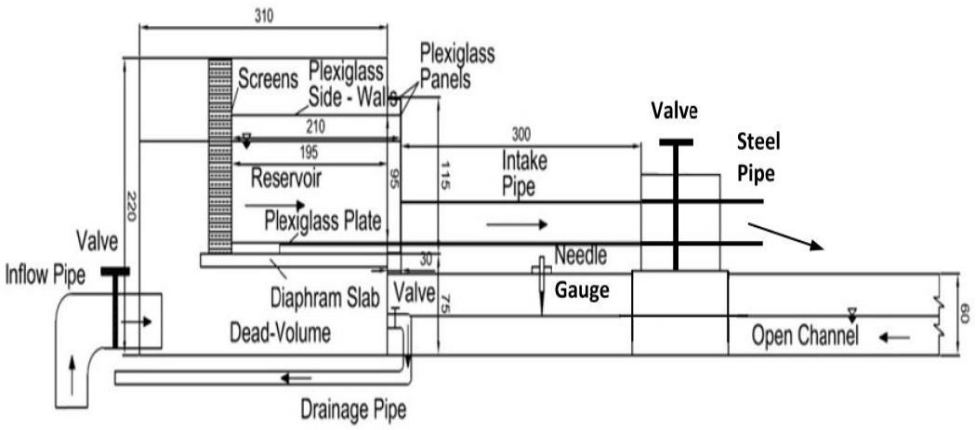

Figure 4.4 Side view of experimental setup of Haspolat (2015)

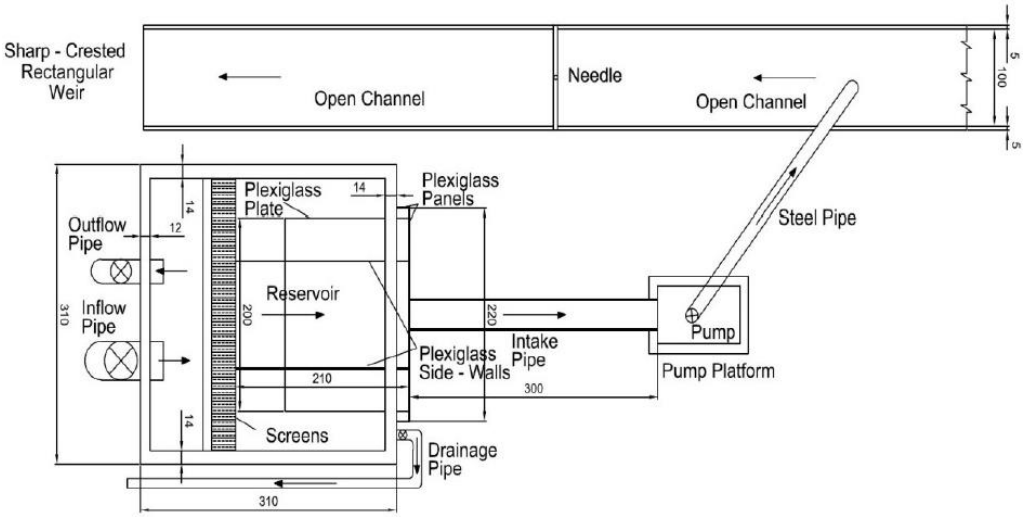

Figure 4.5 Plan view of experimental setup of Baykara (2013)

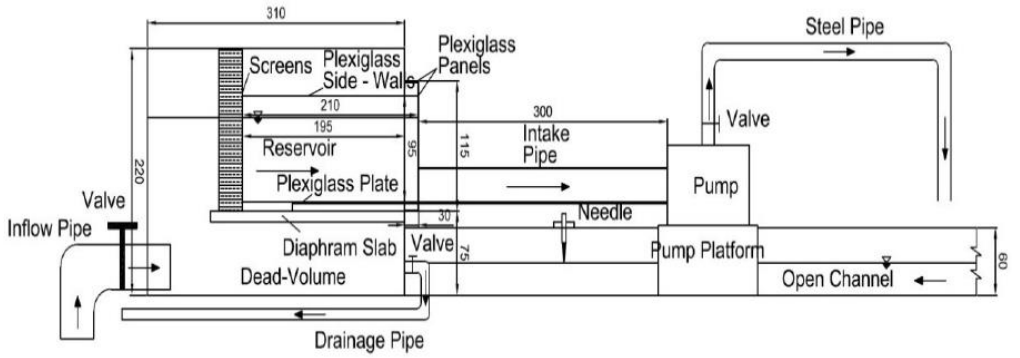

Figure 4.6 Plan view of experimental setup of Baykara (2013)

As a result, in this study similar to Haspolat (2015), for the similar pipe diameters the discharge values are lower resulting in lower vortex strengths compared to Baykara (2013). As mentioned above, higher discharge leads to higher critical submergence depths. Comparison between gravity and pumped flow for similar geometries are given below in Table 4.1.

Table 4.1 Comparison of similar setups with different discharge values between Tataroğlu (2014) and this study

						Experiment	Simulation
Model Name	D (cm)	b_{left} (cm)	b_{right} (cm)	Q (l/s)	Solver	S_c (cm)	S_c (cm)
Tataroğlu (2014)	10.00	20.00	20.00	51.65	LES	66.50	41.50
Case 13	10.00	20.00	30.00	16.64	LES	15.10	12.50

Lower discharge values with respect to pipe diameter lead difficulties in visualizing a full air-core vortex up to entrance of the intake pipe by air-water interface. Therefore, in order to be able to capture the air-core vortex, finer grid size had to be used in the present study compared to the numerical study of Tataroğlu (2014). She used 0.015 m coarse and 0.0075 fine mesh size in the two mesh blocks used in her simulations. On the other hand, in this study 0.015 m coarse mesh size and 0.003 m fine mesh size is used. Even if more grid points are used in this study, Tataroğlu (2014) observed a larger portion of air-entraining vortex by plotting visual air-water interface due to the effect of pumped flow against gravity flow. Hence, circulation values and vorticity contours are used to follow the tail of the vortex formation in the present study.

4.4 Effect of Sidewall Clearance

Assuming that $b_{left} < b_{right}$ and keeping b_{left} and discharge constant, once b_{right} is increased, asymmetry level increases. In this description if $b_{left} > 1.5D$, as the asymmetry level increases, S_c slightly increases (compare cases 6, 8, 9 and 10, 11). There is one exception to that which is case 15 (compare cases 13, 14, 15). On the other hand, if $b_{left} < 1.5D$, as the asymmetry level increases, S_c slightly decreases (compare cases 3, 4, 5). However, more simulations are needed to strengthen this idea.

4.4 Prototype Analysis

To observe the scale effect, case 13 with the smallest reservoir size and mesh size which costed the least computational time is selected for the prototype analysis. Case 13 which has a 10 cm pipe diameter, 20 cm left and 30 cm right sidewall clearance are remodeled with 1/10 length ratio. All dimensions are enlarged by 10 times including the step size (Δh_s) which becomes 0.25 m. By using the Froude similitude, discharge value of prototype is recalculated for case 13. Mesh size does not change for prototype case. Due to the scale effect, the critical submergence depth of the prototype case is expected to be higher than the value obtained by enlarging the critical submergence depth of the case 13 by 10. Case 13 and the enlarged values for the prototype scale are shown below in Table 4.2.

Table 4.2 Parameters of Case 13 and the corresponding prototype scale

Case Parameters				
Case No	**D** (cm)	$\mathbf{b}_{left}$ (cm)	$\mathbf{b}_{right}$ (cm)	**Q (l/s)**
13	10.00	20.00	30.00	16.64
Prototype	100.00	200.00	300.00	5,260.00

It is expected that the critical submergence depth of the prototype scale should be 1.25 m or higher, correspondingly the reservoir water depth should be 2.25 or higher. However, running the simulation with this water depth even a single weak dimple is not observed. On the contrary, simulations are repeated with lower reservoir water depths but the results did not change. Due to the gravity flow, it was already hard to observe the vortex formation for the model cases, in addition to that, mesh size is not enough to visualize a vortex core which is getting thinner towards the intake pipe.

Even if the number of grid points in the coarse and fine mesh blocks are increased approximately 8 times, an air-entraining vortex cannot be observed

for 2.50 m, 2.25 m and 2.00 m reservoir water depths. Only weak dimples are observed such as shown in Figure 4.7.

Each prototype scale run reserves approximately 200 gb space and has about 10-day computational time which means further increasing the number of grid points will lead to a very expensive solution. As a result, it was decided that at low discharge values it is not feasible to make a prototype scale analysis. Since, the vortex core is getting thinner and weaker, use of a finer grid is required.

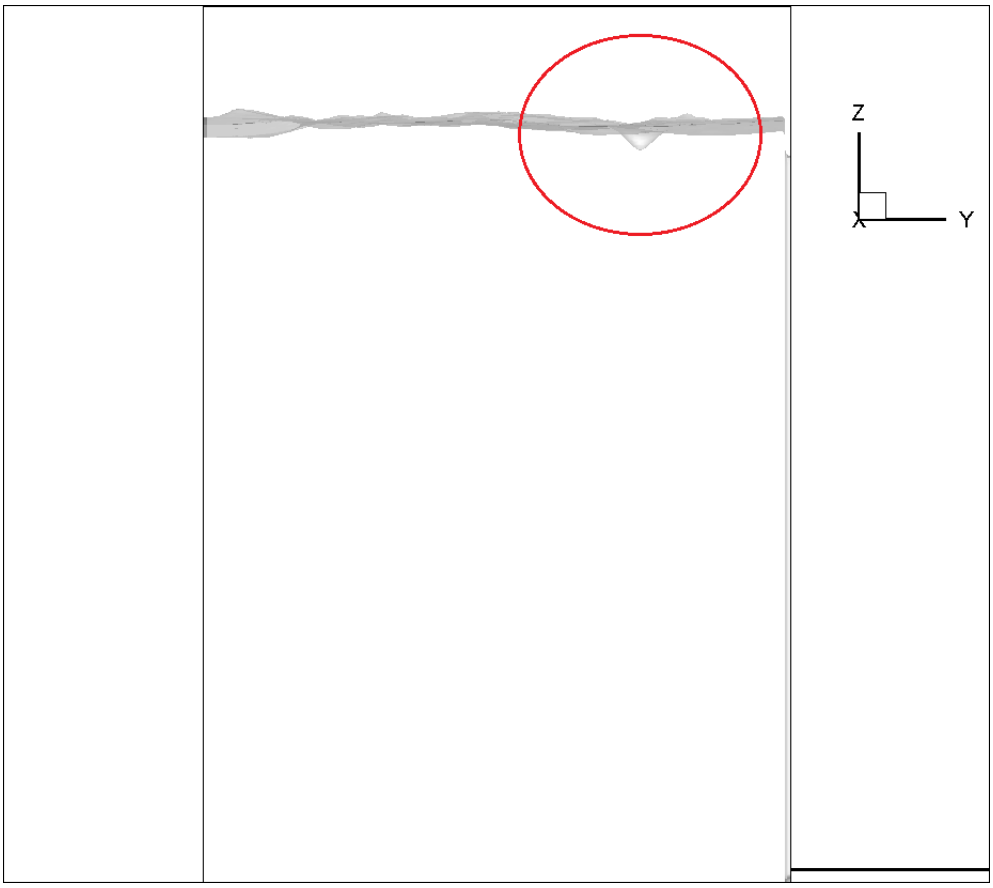

Figure 4.7 Weak dimple observed in the prototype scale simulation

4.5 Comparison between Numerical and Experimental Results

The main purpose of this study is to compare the experimental and numerical results and test the accuracy of the numerical simulations in investigating vortex formation at horizontal intakes.

The critical submergence depths (S_c), reservoir water depths (h) and circulation values (Γ) of the experiments and corresponding simulations are given in Table 4.3 for different cases investigated.

$\Gamma = \iint w_z \, . \, dA$;

where w_z is vertical vorticity and dA is per unit area which is taken around an infinitesimal loop. Circulation values are obtained by integration of vertical vorticity over vortex core area.

Circulation values are calculated for different horizontal planes taken from vortex core and they are roughly the same. This means, circulation value of vortex core does not change between free water surface and intake pipe.

Also, the results of numerical simulations are compared with the past studies of Gordon (1970) and Reddy and Pickford (1972) in Table 4.3. As it can be seen in this table the most commonly used empirical equations in practice give much more higher critical submergence levels compared to the experimental and numerical results.

Table 4.3 Comparison of the experimental and numerical results

Case Parameters					Experiments		Numerical Simulations				Gordon (1970)		Reddy & Pickford (1972)	
No	D (cm)	b_{left} (cm)	b_{right} (cm)	Q (lt/s)	S_c-exp (cm)	S_c/D	S_c (cm)	S_c/D	h (cm)	Γ	S_c (cm)	S_c/D	S_c (cm)	S_c/D
1	25.00	20.00	60.00	45.03	14.10	0.564	10.00	0.40	35.00	-3.82E-02	33.26	1.33	39.65	1.59
2	25.00	20.00	70.00	41.66	11.60	0.464	10.00	0.40	35.00	-3.11E-02	30.76	1.23	38.55	1.54
3	25.00	30.00	50.00	46.75	18.60	0.744	17.50	0.70	42.50	-2.83E-02	34.50	1.38	40.20	1.61
4	25.00	30.00	60.00	46.75	19.10	0.764	17.50	0.70	42.50	-3.07E-02	34.50	1.38	40.20	1.61
5	25.00	30.00	70.00	46.75	17.90	0.716	15.00	0.60	40.00	2.40E-02	34.50	1.38	40.20	1.61
6	25.00	40.00	50.00	50.27	17.60	0.704	15.00	0.60	40.00	-2.70E-02	37.11	1.48	41.35	1.65
7	25.00	40.00	50.00	50.27	17.60	0.704	15.00	0.60	40.00	-2.61E-02	0.00	0.00	25.00	1.00
8	25.00	40.00	60.00	51.17	20.60	0.824	17.50	0.70	42.50	-2.59E-02	37.80	1.51	41.65	1.67
9	25.00	40.00	70.00	52.98	26.90	1.076	17.50	0.70	42.50	-3.05E-02	39.16	1.57	42.25	1.69
10	25.00	50.00	60.00	46.75	18.90	0.756	15.00	0.60	40.00	2.15E-02	34.50	1.38	40.20	1.61
11	25.00	50.00	70.00	44.18	19.70	0.788	17.50	0.70	42.50	2.45E-02	32.63	1.31	39.38	1.58
12	25.00	60.00	70.00	49.38	21.40	0.856	17.50	0.70	42.50	-2.03E-02	36.49	1.46	41.08	1.64
13	10.00	20.00	30.00	16.64	15.10	1.51	12.50	1.25	22.50	-1.61E-02	48.58	4.86	31.40	3.14
14	10.00	20.00	40.00	17.23	14.70	1.47	12.50	1.25	22.50	2.17E-02	50.30	5.03	32.16	3.22
15	10.00	20.00	50.00	16.64	13.20	1.32	10.00	1.00	20.00	2.91E-02	48.58	4.86	31.40	3.14
16	10.00	30.00	40.00	17.84	23.90	2.39	12.50	1.25	22.50	-1.91E-02	52.07	5.21	32.94	3.29
17	10.00	30.00	50.00	22.92	22.30	2.23	20.00	2.00	30.00	-1.71E-02	66.94	6.69	39.49	3.95
18	10.00	40.00	50.00	22.92	25.20	2.52	20.00	2.00	30.00	-1.25E-02	66.94	6.69	39.49	3.95
19	10.00	50.00	60.00	28.47	25.80	2.58	22.50	2.25	32.50	1.53E-02	83.10	8.31	46.61	4.66

As mentioned earlier, 2.50 cm increment (Δh_s) is used in changing the reservoir water depth. It is an important parameter affecting comparison of experimental and numerical results, because there could be another vortex formation within this 2.50 cm range. Hence, 2.50 cm is added to all critical submergence depths of the numerical cases and shown as an additional bar below in Figure 4.8 to visualize the error range.

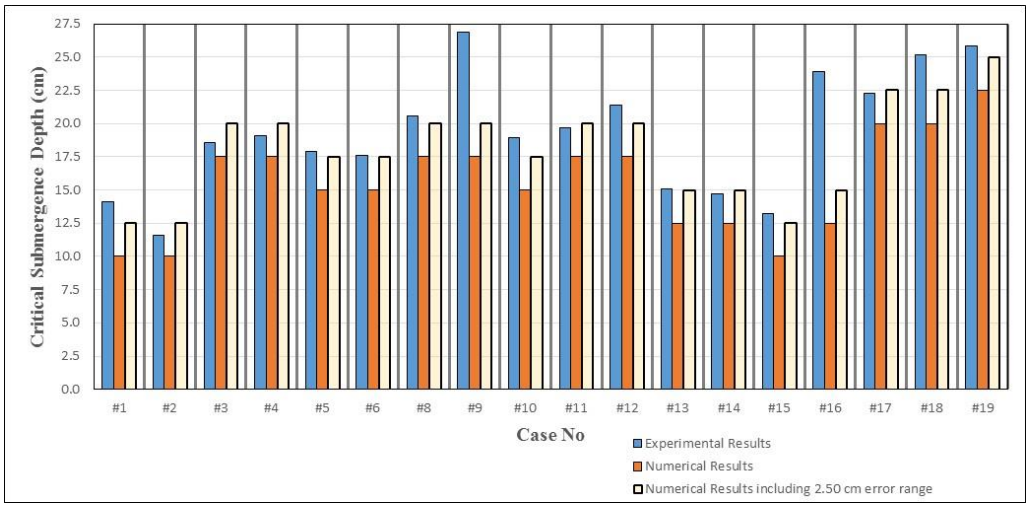

Figure 4.8 Critical submergence depths of the experimental and numerical cases

As seen, the results of numerical simulations are very close to the experimental results except the two outlier cases which are cases 9 and 16. There might be a problem with these two cases in the experiments. The critical submergence depths of the experimental case 9 and 16 are very higher compared to similar experimental cases with similar discharge values. Hence, these two cases are taken out from data set.

Even if the results are very close, experimental results are barely higher than numerical results for all cases.

The error margin between experiments and numerical simulations are calculated below at Table 4.4.

Table 4.4 Error margins for the numerical results

Case Parameters					Physical Experiment	Numerical Simulations	Error Margins (%)	
No	D (cm)	b_l (cm)	b_r (cm)	Q (l/s)	S_c-exp (cm)	S_c (cm)	max	min
1	25.00	20.00	60.00	45.03	14.100	10.000	29.08	11.35
2	25.00	20.00	70.00	41.66	11.600	10.000	13.79	0.00
3	25.00	30.00	50.00	46.75	18.600	17.500	5.91	0.00
4	25.00	30.00	60.00	46.75	19.100	17.500	8.38	0.00
5	25.00	30.00	70.00	46.75	17.900	15.000	16.20	2.23
6	25.00	40.00	50.00	50.27	17.600	15.000	14.77	0.57
8	25.00	40.00	60.00	51.17	20.600	17.500	15.05	2.91
10	25.00	50.00	60.00	46.75	18.900	15.000	20.63	7.41
11	25.00	50.00	70.00	44.18	19.700	17.500	11.17	0.00
12	25.00	60.00	70.00	49.38	21.400	17.500	18.22	6.54
13	10.00	20.00	30.00	16.64	15.100	12.500	17.22	0.66
14	10.00	20.00	40.00	17.23	14.700	12.500	14.97	0.00
15	10.00	20.00	50.00	16.64	13.200	10.000	24.24	5.30
17	10.00	30.00	50.00	22.92	22.300	20.000	10.31	0.00
18	10.00	40.00	50.00	22.92	25.200	20.000	20.63	10.71
19	10.00	50.00	60.00	28.47	25.800	22.500	12.79	3.10
						Average:	**16.76**	**3.21**

Individually, the maximum error is 29.08% for case 1 and the minimum error is 0.00% for cases 2, 3, 4, 11, 14 and 17. Also, the maximum average error is 16.76% and the minimum average error is only 3.21%. As a result, it can be said that numerical simulations are reliable to observe visible vortex and decide the critical submergence depth for industrial use. Moreover, with a finer mesh options, the found error margin might decrease.

CHAPTER 5

CONCLUSIONS

In the present study, Haspolat's (2015) physical experiments are numerically modelled and simulated with Flow 3D to investigate vortex formation at asymmetrical intake structures. The critical submergence depths of experimental and numerical results are compared to evaluate the accuracy of numerical simulations. Large Eddy Simulation (LES) model is used for all cases. As an outcome of this numerical study, the following conclusions can be obtained:

1. Since the average error between 3.21% - 16.76%, Flow 3D is a reliable software to observe vortex formations at horizontal intakes. Numerical simulations are less time consuming and appropriate for industrial use instead of physical experiments.

2. Water depth increment (Δh_s) is taken as 2.50 cm for the simulations and the average error margin for critical submergence depth is found within a range of 3.21% - 16.76%. Error margin could be lowered by reducing the mesh size. This would increase the computation time, however, for real structural systems, error margin might be closer to the physical experiments.

3. 10~15 minutes observation time was used in the physical experiments. On the contrary, only 50 seconds time interval is selected in the present study because of the long run times. It is possible to obtain better agreement with the experimental results if longer simulation times are used.

4. Gravity was the driving force in the experiments simulated within this study, where it was not possible to visualize a full air-core vortex towards the intake pipe. On the other hand, in the study of Tataroğlu (2014), formation of the air-entraining vortices was investigated for pumped flow systems where a larger portion of the air-core vortex was visualized. Therefore, it can be concluded that pumped flow systems are more suitable than gravity driven flows to observe the air-entraining vortex in the numerical simulations conducted with Flow-3D software.
5. As the vortex is very small for gravity flows, especially in the prototype scale, it was not possible to capture the air-core vortex.

For future studies, numerical studies can be extended out of the range of experimental studies using Flow3D software to investigate the effect of, Froude number or asymmetry level on critical submergence depth.

REFERENCES

Anwar, H.O. (1968), "Prevention of Vortices at Intakes", Water Power 1968(10), 393-401.

Baykara, A. (2013), "Effect of Hydraulic Parameters on the Formation of Vortices at Intake Structures", M.Sc. Thesis, Civil Engineering Dept., Middle East Technical University.

Beale, J.T. and Majda, A. (1982a), "Vortex methods I: Convergence in Three Dimensions", Mathematics of Computation, Vol. 39, No. 159, 1-27.

Beale, J.T. and Majda, A. (1982b), "Vortex methods II: Higher Order Accuracy in Two and Three Dimensions", Mathematics of Computation, Vol. 39, No. 159, 29-52.

Chen, Y., Wu, C., Wang, B. and Du, M. (2012), "Three-dimensional Numerical Simulation of Vertical Vortex at Hydraulic Intake", 2012 International Conference on Modern Hydraulic Engineering, March 9-11, Nanjing, Jiangsu Province, China.

Chorin, A.J. (1973), "Numerical Study of Slightly Viscous Flow", Journal of Fluid Mechanics, 57, 785-796.

Chorin, A.J. (1982), "The Evolution of a Turbulent Vortex", Communications in Mathematical Physics, 83, 517-535.

Durgin, W.W. and Hecker, G.E. (1978), the Modeling of Vortices in Intake Structures. Proc IAHR-ASME-ASCE Joint Symposium on Design and Operation of Fluid Machinery, CSU Fort Collins, June 1978 vols I and III.

Flow Science Inc., www.flow3d.com, last visited on August 2017.

Gordon, J.L. (1970), “Vortices at Intakes”, Water Power 1970(4), 137-138.

Göğüş, M., Köken M., Baykara A. (2016), “Formation of Air-entraining Vortices at Horizontal Intakes without approach flow induced circulation”, Journal of Hydrodynamics, Vol. 28, Iss. 1, 102-113.

Gürbüzdal, F. (2009), “Scale Effects on the Formation of Vortices at Intake Structures”, M.Sc. Thesis, Civil Engineering Dept., Middle East Technical University.

Hald, O. (1979), “Convergence of Vortex Methods for Euler’s Equations. II”, SIAM Journal on Numerical Analysis, Vol. 16, No. 5, 726-755.

Hald, O. and Del Prete V.M. (1978), “Convergence of Vortex Methods for Euler’s Equations”, Mathematics of Computation, Vol. 32, No. 143, 791-809.

Haspolat, E. (2015), “Determination of Critical Submergence Depth at Horizontal Intakes”, M.Sc. Thesis, Civil Engineering Dept., Middle East Technical University.

Hirt, C.W., Nichols, B.D. (1981), “Volume of Fluid (VOF) Method for the Dynamics of Free Boundaries”, Journal of Computational Physics, Vol. 39, Iss. 1, 201-225.

Knauss, J. (1987), “Swirling Flow Problems at Intakes”, A.A. Balkema, Rotterdam.

Kolmogorov, A. (1941), “The Local Structure of Turbulence in Incompressible Viscous Fluid for Very Large Reynolds’ Numbers”, Doklady Akademiia Nauk SSSR, Vol.30, 301-305.

Li, H., Chen, H., Ma, Z. and Zhou, Y. (2008), “Experimental and Numerical Investigation of Free Surface Vortex”, Journal of Hydrodynamics, 20(4), 485-491.

Moore, D.W. (1971), “The Discrete Vortex Approximation of a Finite Vortex Sheet”, California Inst. Of Tech. Report AFOSR-1804-69.

Nagahara, T., Sato, T., Okamura, T., Iwano, R. (2003), “Measurement of the Flow around the Submerged Vortex Cavitation in a Pump Intake by Means of PIV”, Fifth International Symposium on Cavitation (cav2003), Osaka, Japan, November 1-4.

Nakayama, A. and Hisasue, N. (2010), “Large Eddy Simulation of Vortex Flow in Intake Channel of Hydropower Facility”, Journal of Hydraulic Research, Vol.48, Iss. 4., 415-427.

Okamura, T., Kyoji, K. and Jun, M. (2007), “CFD Prediction and Model Experiment on Suction Vortices in Pump Sump”, The 9th Asian International Conference on Fluid Machinery, October 16-19, Jeju, Korea.

Reddy, Y.R. and Pickford, J.A. (1972), “Vortices at Intakes in Conventional Sumps”, Water Power 1972(3), 108-109.

Rosenhead, L. (1931), “The Formation of Vortices from a Surface of Discontinuity”, Proc. Roy. Soc. London Series A, Containing Papers of a Mathematical and Physical Character, Vol. 134, Iss. 823, 170-192.

Sarkardeh, H., Zarrati, A.R., Jabbari, E. and Marosi, M. (2014), “Numerical Simulations and Analysis of Flow in a Resorvoir in the Presence of Vortex”, Engineering Applications of Computational Fluid Mechanics, Vol. 8, Iss. 4, 598-608.

Sarkardeh, H., Zarrati, A.R., Roshan, R. (2010), “Effect of Intake Head Wall and Trash Rack on Vortices”, Journal of Hydraulic Research, Vol. 48, Iss. 1, 108-112.

Takami, H. (1964), “Numerical Experiment with Discrete Vortex Approximation, with Reference to the Rolling Up of a Vortex Sheet”, Dept. of Aero. and Astro., Stanford University Report SUDAER 202.

Tataroğlu, R.M. (2014), “Numerical Investigation of Vortex Formation at Intake Structures Using Flow 3D Software”, M.Sc. Thesis, Civil Engineering Dept., Middle East Technical University.

Taştan, K. and Yıldırım, N. (2010), “Effects of Dimensionless Parameters on Air-entraining Vortices”, Journal of Hydraulic Research, Vol. 48, Iss. 1, 57-64.

Yıldırım, N. and Kocabaş, F. (1995), “Critical Submergence for Intakes in Open Channel Flow”, Journal of Hydraulic Engineering, ASCE, Vol. 121, Iss. 12, 900-905.

Zhao, L.J. and Nohmi, M. (2012), “Numerical Simulation of Free Water Surface in Pump Intake”, IOP Conference Series: Earth and Environmental Science, Vol. 15, Part 5.

APPENDICES

A. RESULTS OF NUMERICAL SIMULATIONS

Case 1: D = 25.00 cm, b_{left} = 20.00 cm, b_{right} = 60.00 cm, Q = 45.03 l/s

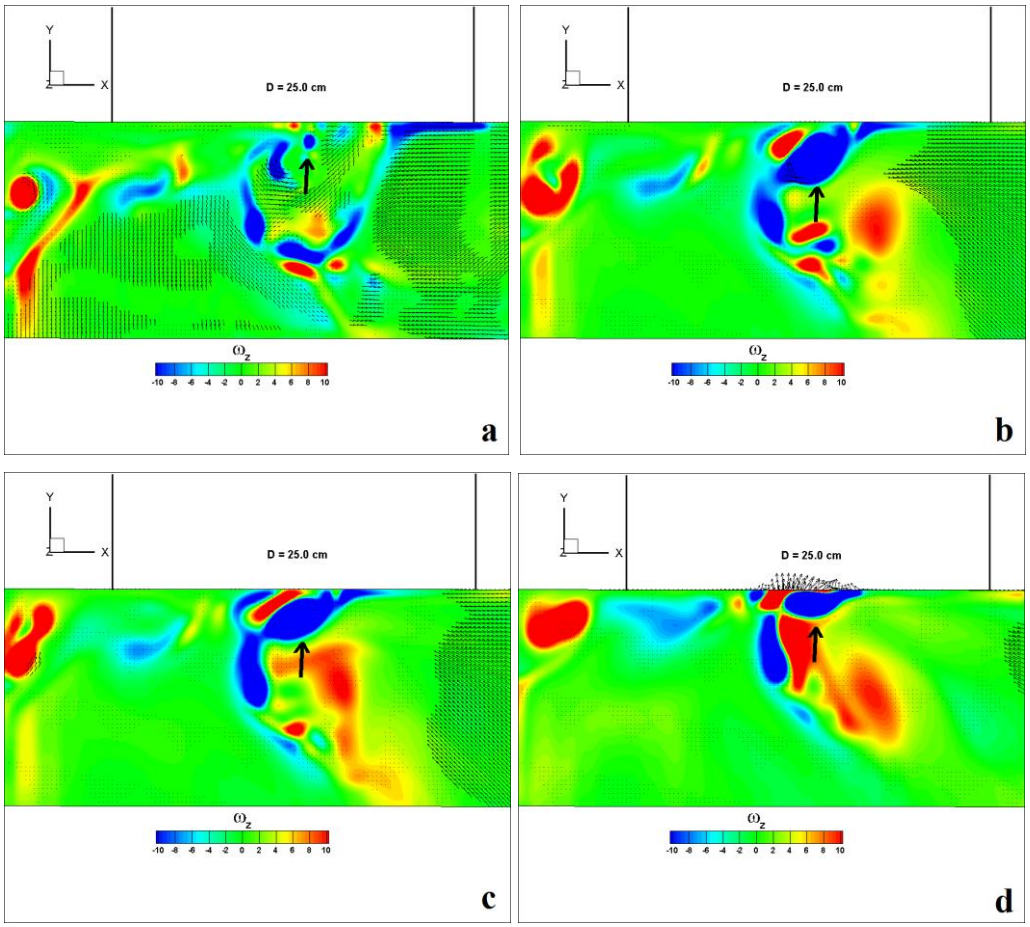

Figure A.1 Case 1: Vertical vorticity contours (ωz, 1/sec) at: a) free water surface; b) just below the visible vortex core; c) mid-S_c level, (h = 35.00 cm); d) top point of intake

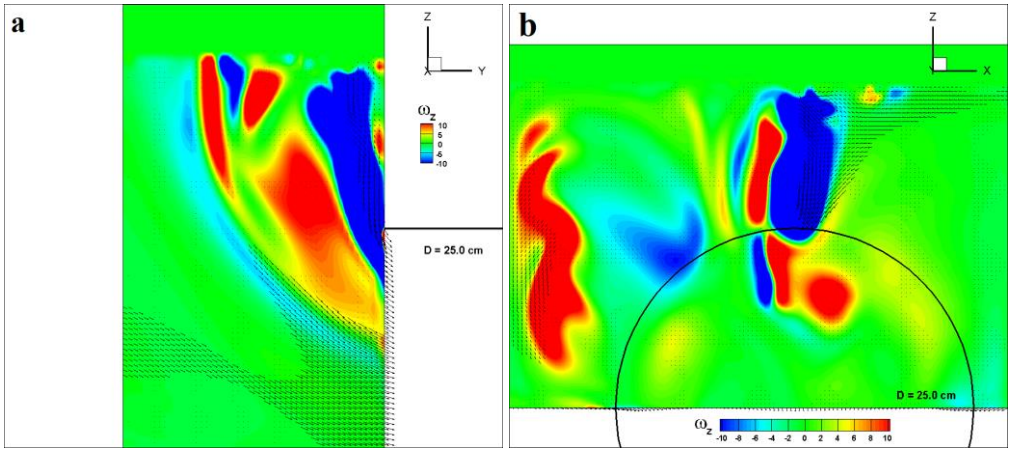

Figure A.2 Case 1: Vorticity contours around z-axis (ω_z, 1/sec): a) longitudinal cross section; b) transverse cross section

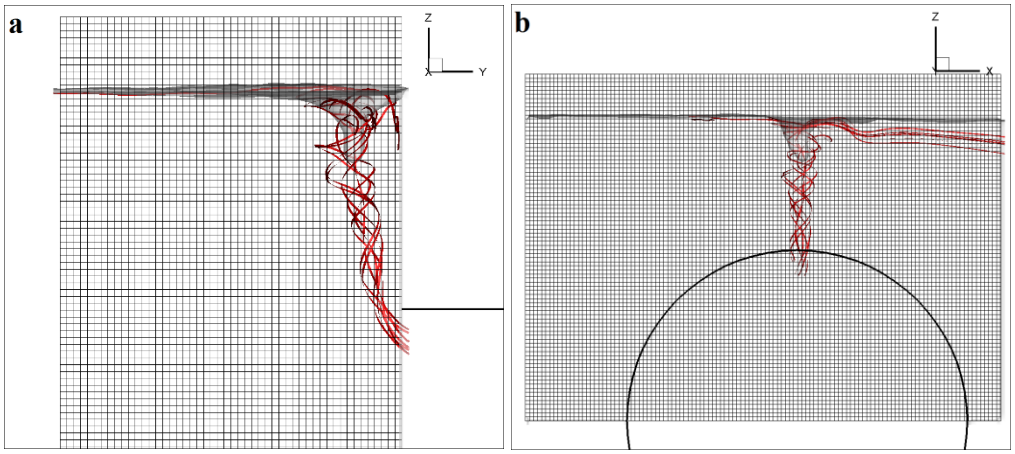

Figure A.3 Case 1: Air-water interface isosurfaces together with the 3D streamlines: a) longitudinal cross section; b) transverse cross section

Case 2: D = 25.00 cm, b_{left} = 20.00 cm, b_{right} = 70.00 cm, Q = 41.66 l/s

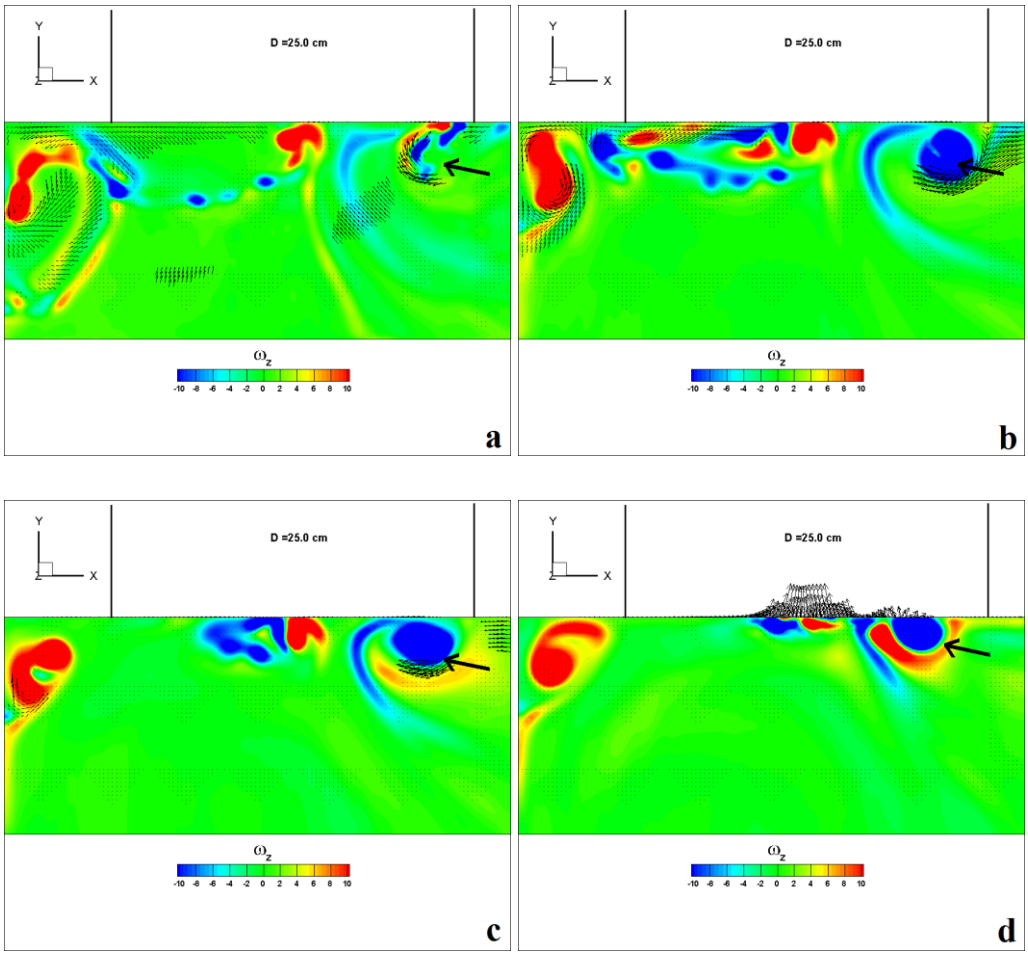

Figure A.4 Case 2: Vertical vorticity contours (ωz, 1/sec) at: a) free water surface; b) just below the visible vortex core; c) mid-S_c level, (h = 35.00 cm); d) top point of intake

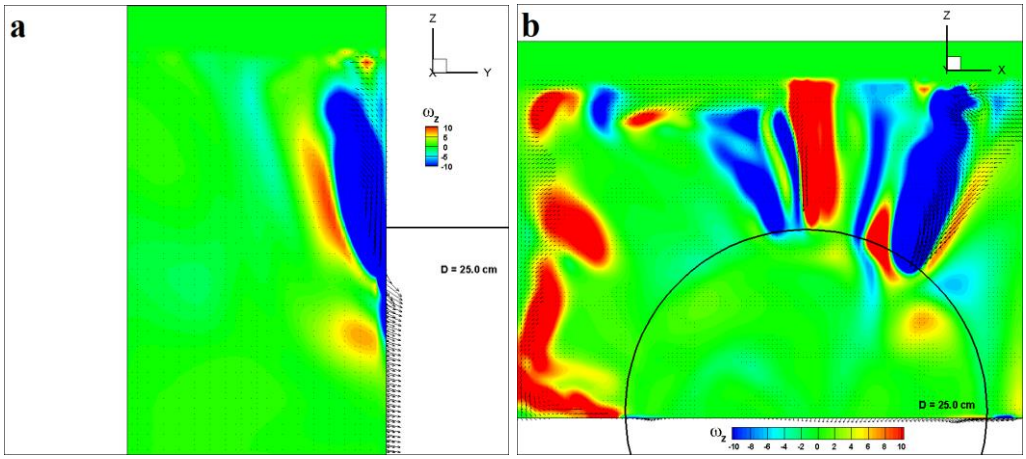

Figure A.5 Case 2: Vorticity contours around z-axis (ω_z, 1/sec): a) longitudinal cross section; b) transverse cross section

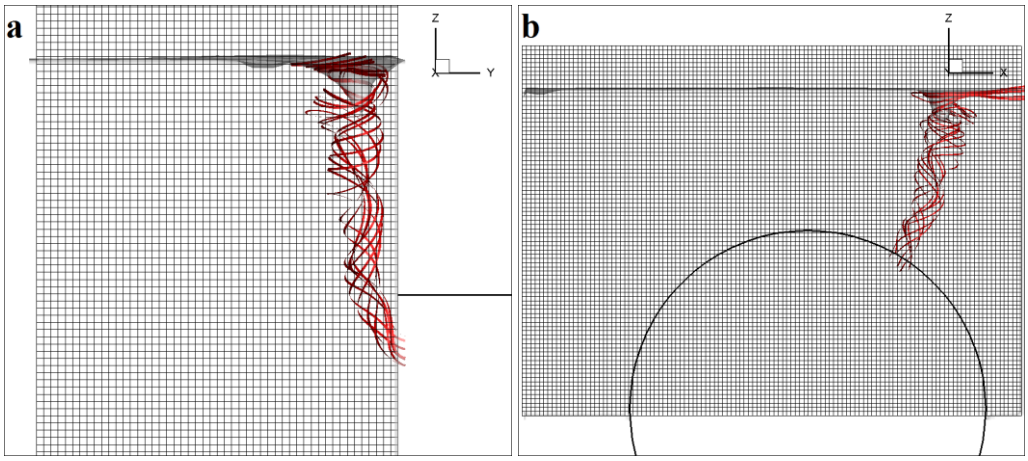

Figure A.6 Case 2: Air-water interface isosurfaces together with the 3D streamlines: a) longitudinal cross section; b) transverse cross section

Case 3: D = 25.00 cm, b_{left} = 30.00 cm, b_{right} = 50.00 cm, Q = 46.75 l/s

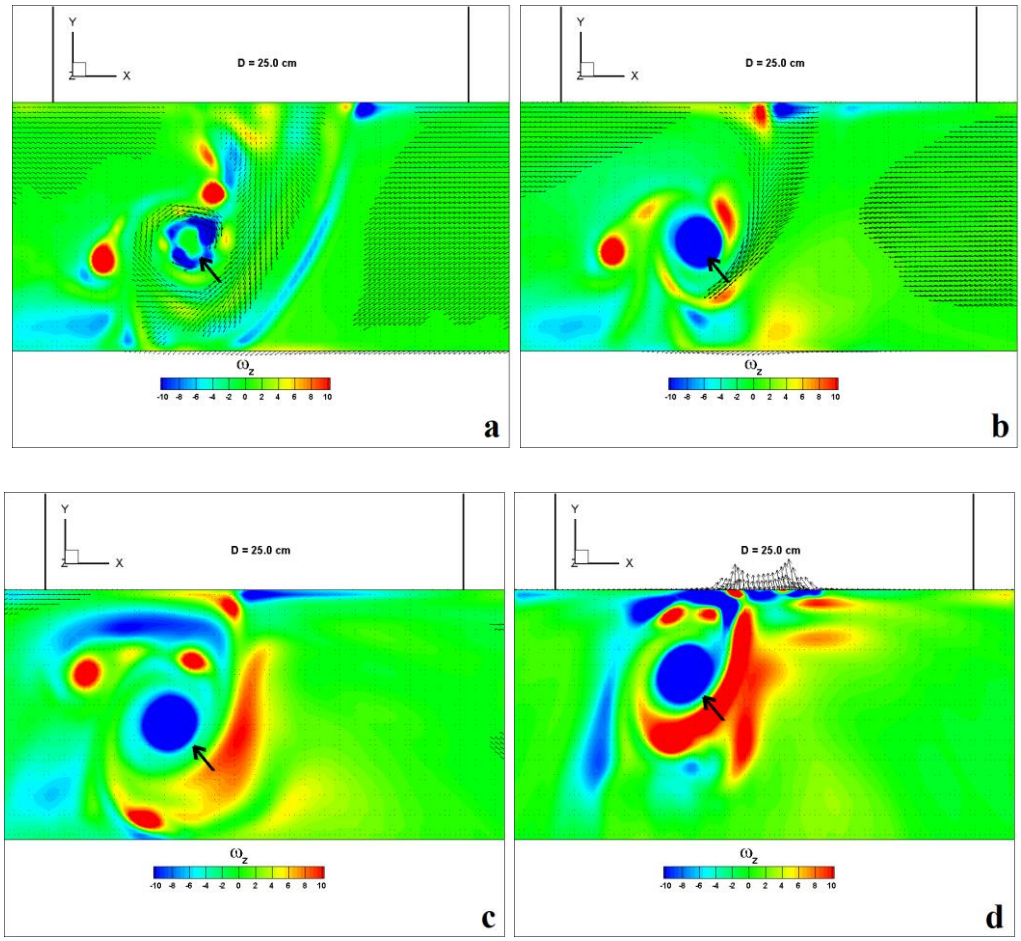

Figure A.7 Case 3: Vertical vorticity contours (ωz, 1/sec) at: a) free water surface; b) just below the visible vortex core; c) mid-S_c level, (h = 42.50 cm); d) top point of intake

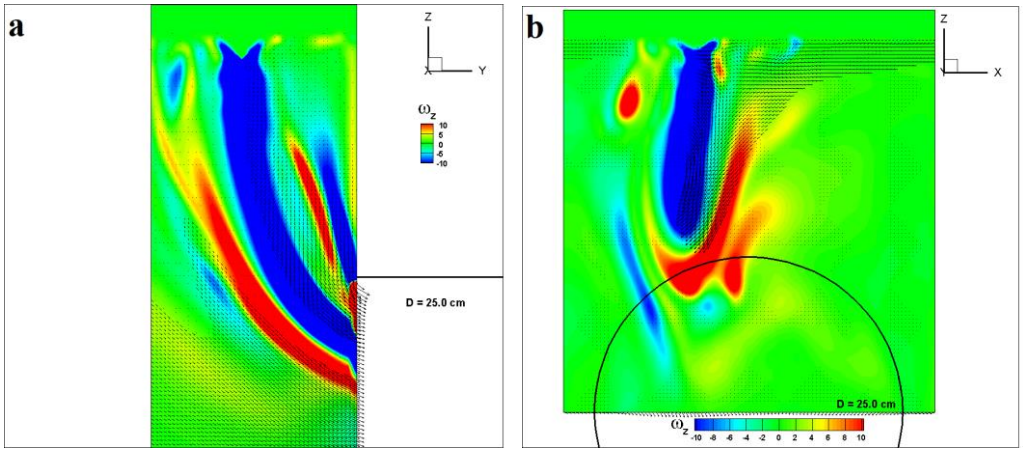

Figure A.8 Case 3: Vorticity contours around z-axis (ω_z, 1/sec): a) longitudinal cross section; b) transverse cross section

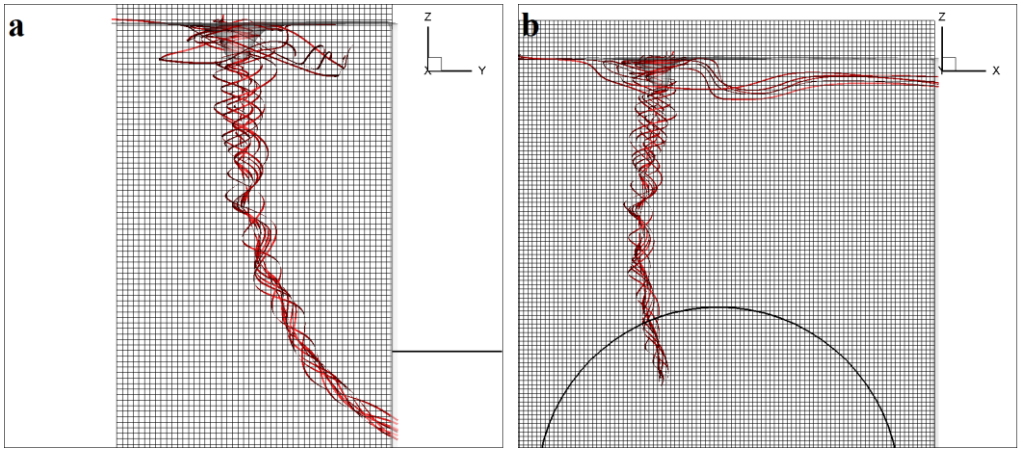

Figure A.9 Case 3: Air-water interface isosurfaces together with the 3D streamlines: a) longitudinal cross section; b) transverse cross section

Case 4: D = 25.00 cm, b_{left} = 30.00 cm, b_{right} = 60.00 cm, Q = 46.75 l/s

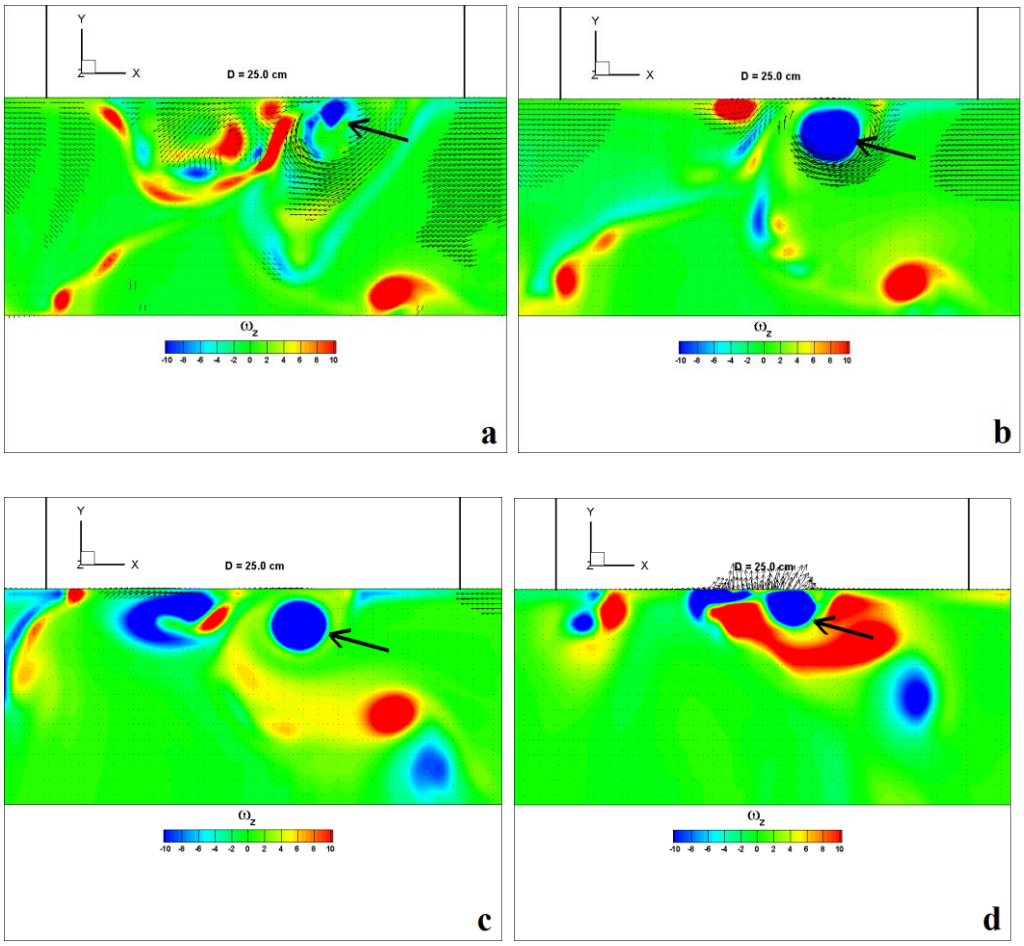

Figure A.10 Case 4: Vertical vorticity contours (ωz, 1/sec) at: a) free water surface; b) just below the visible vortex core; c) mid-S_c level, (h = 42.50 cm); d) top point of intake

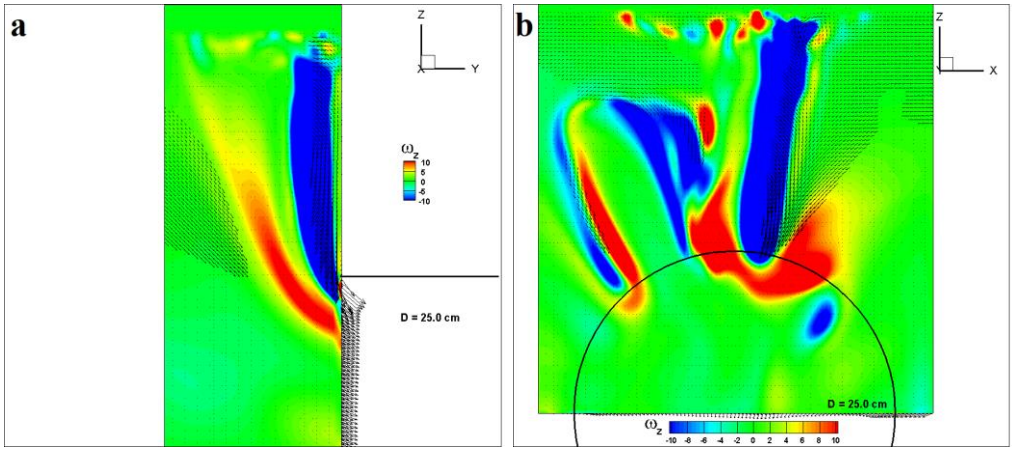

Figure A.11 Case 4: Vorticity contours around z-axis (ω_z, 1/sec): a) longitudinal cross section; b) transverse cross section

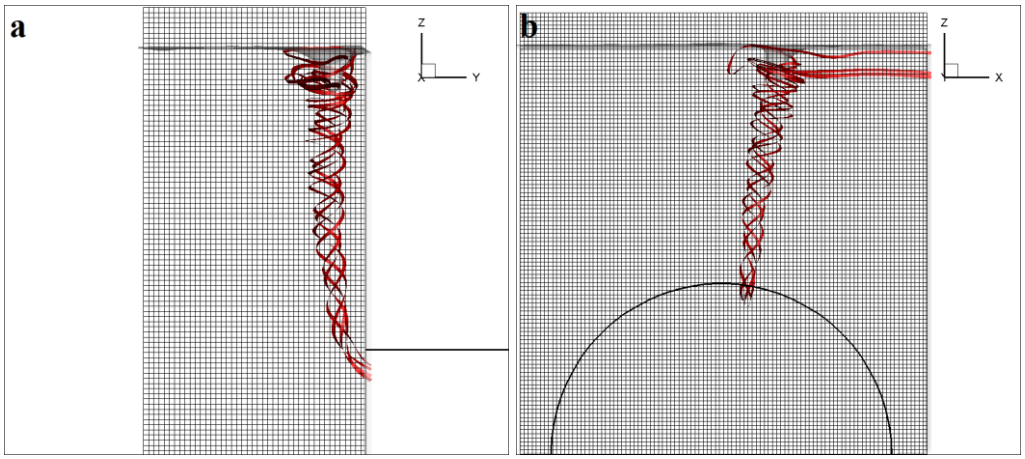

Figure A.12 Case 4: Air-water interface isosurfaces together with the 3D streamlines: a) longitudinal cross section; b) transverse cross section

Case 5: D = 25.00 cm, b_{left} = 30.00 cm, b_{right} = 70.00 cm, Q = 46.75 l/s

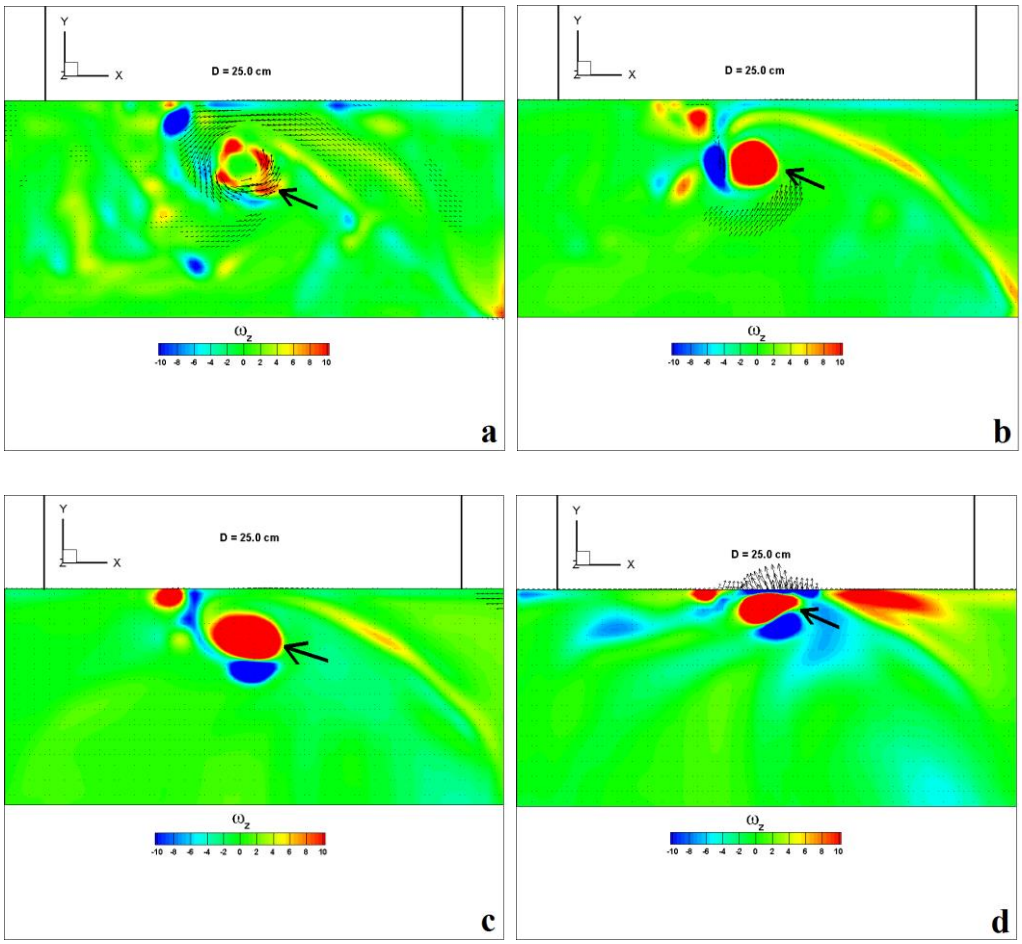

Figure A.13 Case 5: Vertical vorticity contours (ωz, 1/sec) at: a) free water surface; b) just below the visible vortex core; c) mid-S_c level, (h = 40.00 cm); d) top point of intake

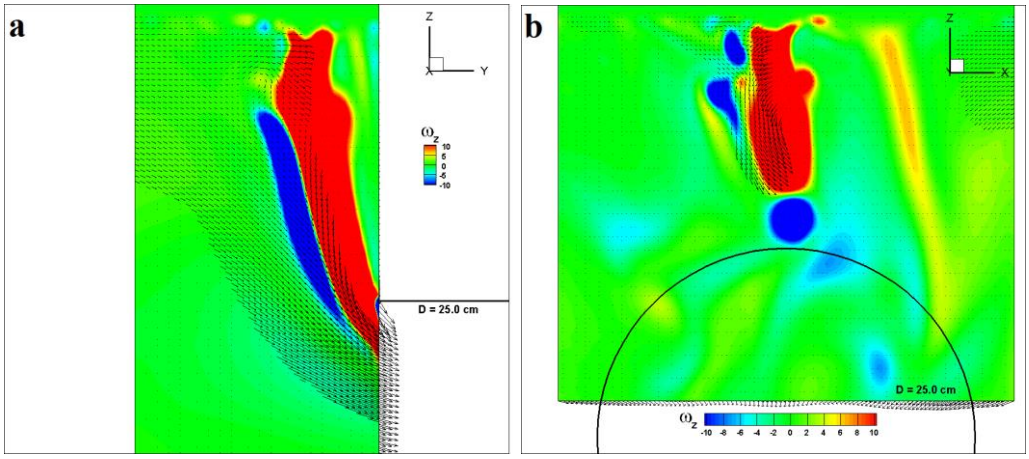

Figure A.14 Case 5: Vorticity contours around z-axis (ω_z, 1/sec): a) longitudinal cross section; b) transverse cross section

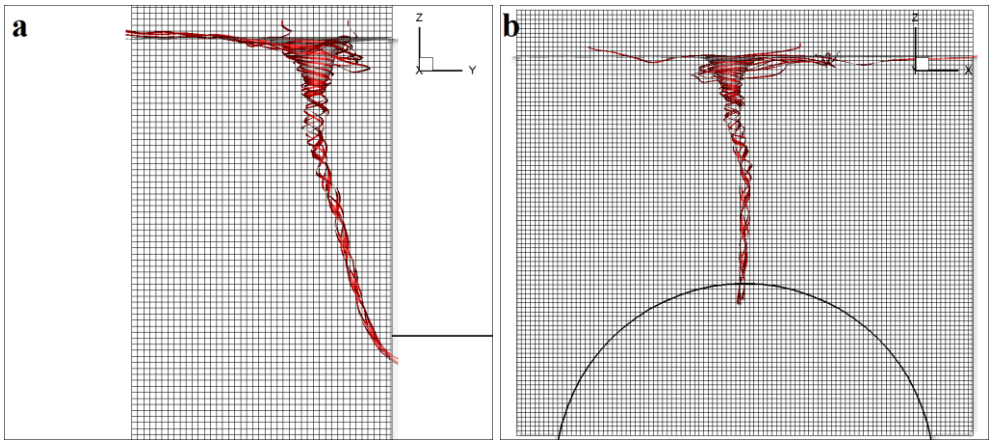

Figure A.15 Case 5: Air-water interface isosurfaces together with the 3D streamlines: a) longitudinal cross section; b) transverse cross section

Case 6: D = 25.00 cm, b_{left} = 40.00 cm, b_{right} = 50.00 cm, Q = 50.27 l/s

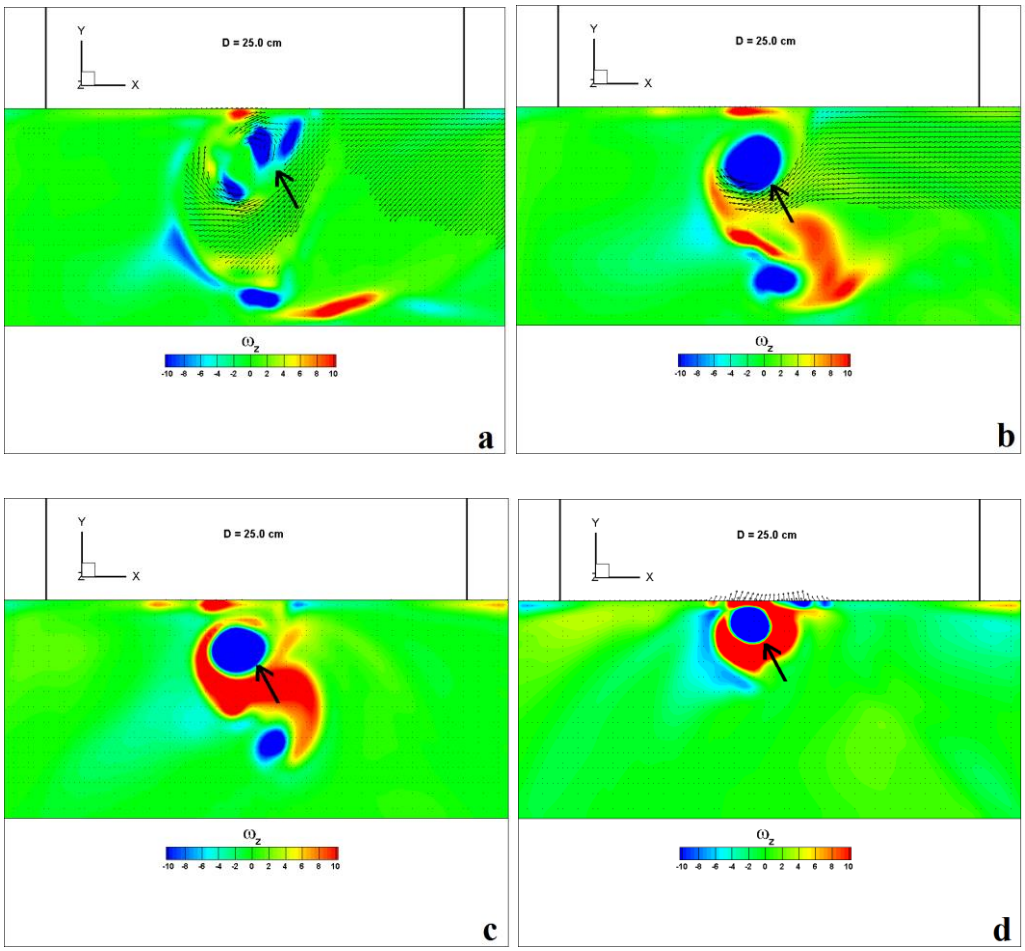

Figure A.16 Case 6: Vertical vorticity contours (ωz, 1/sec) at: a) free water surface; b) just below the visible vortex core; c) mid-S_c level, (h = 40.00 cm); d) top point of intake

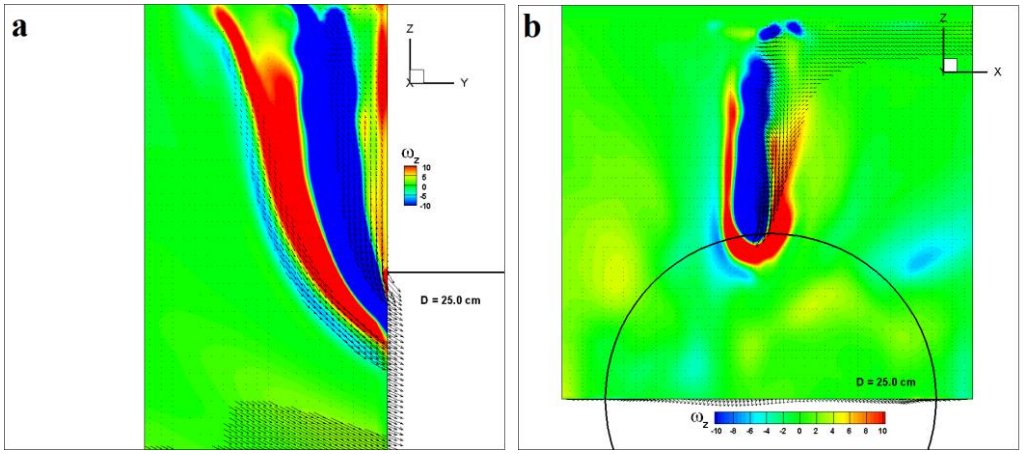

Figure A.17 Case 6: Vorticity contours around z-axis (ω_z, 1/sec): a) longitudinal cross section; b) transverse cross section

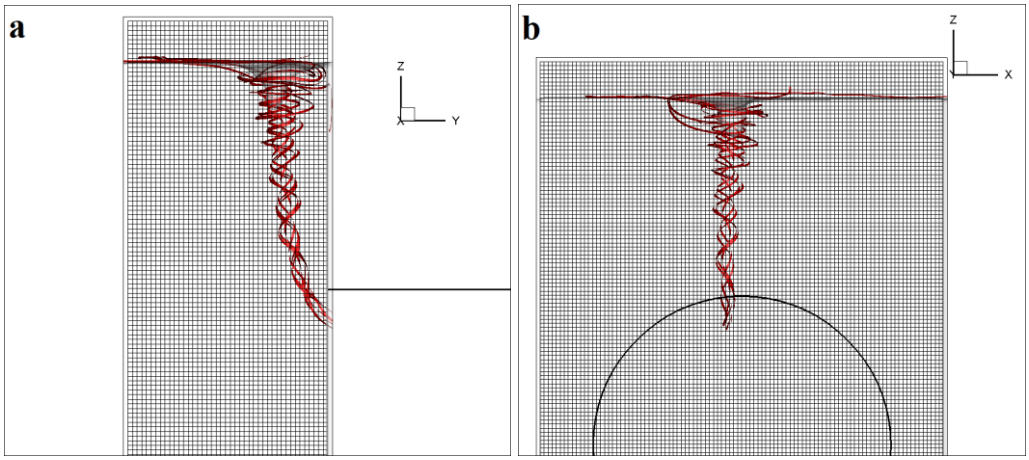

Figure A.18 Case 6: Air-water interface isosurfaces together with the 3D streamlines: a) longitudinal cross section; b) transverse cross section

Case 8: D = 25.00 cm, b_{left} = 40.00 cm, b_{right} = 60.00 cm, Q = 51.17 l/s

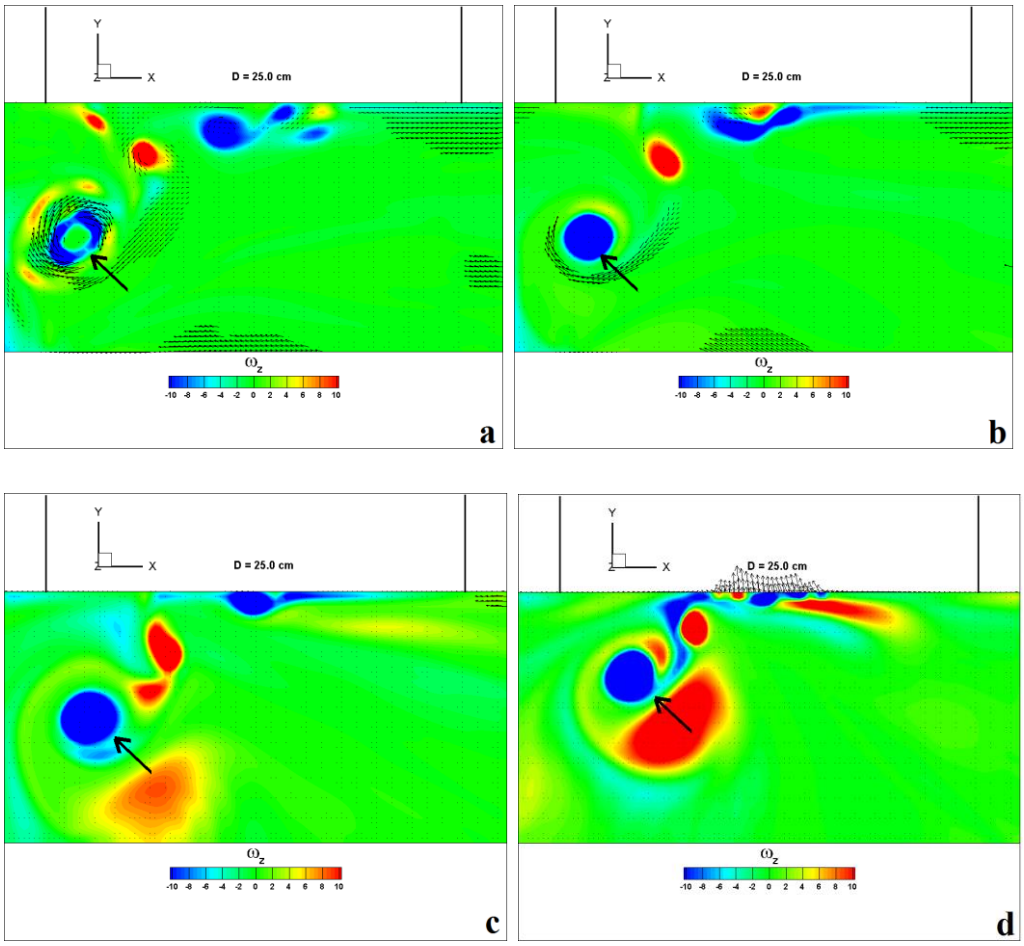

Figure A.19 Case 8: Vertical vorticity contours (ωz, 1/sec) at: a) free water surface; b) just below the visible vortex core; c) mid-S_c level, (h = 42.50 cm); d) top point of intake

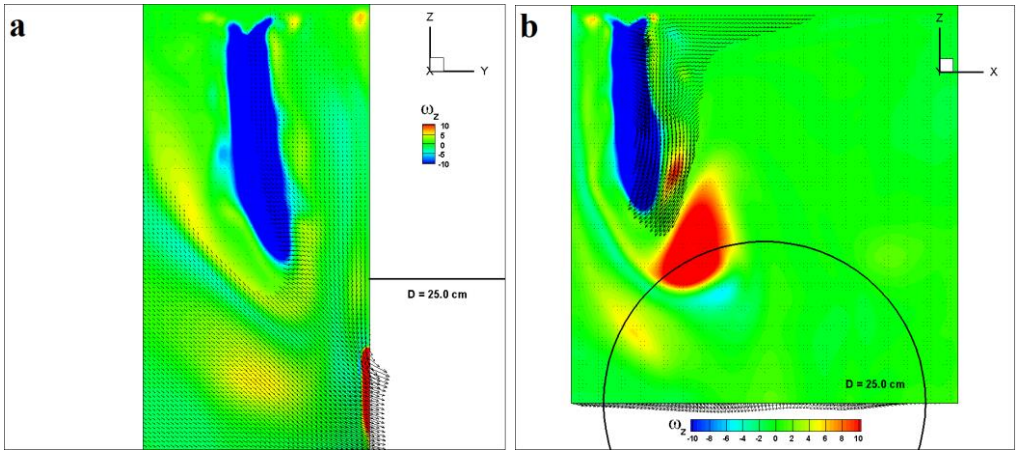

Figure A.20 Case 8: Vorticity contours around z-axis (ω_z, 1/sec): a) longitudinal cross section; b) transverse cross section

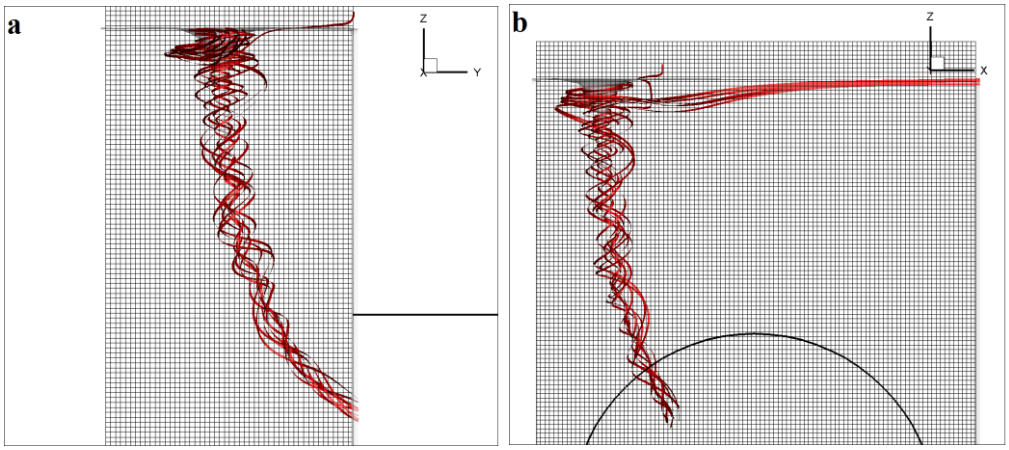

Figure A.21 Case 8: Air-water interface isosurfaces together with the 3D streamlines: a) longitudinal cross section; b) transverse cross section

Case 9: D = 25.00 cm, b_{left} = 40.00 cm, b_{right} = 70.00 cm, Q = 52.98 l/s

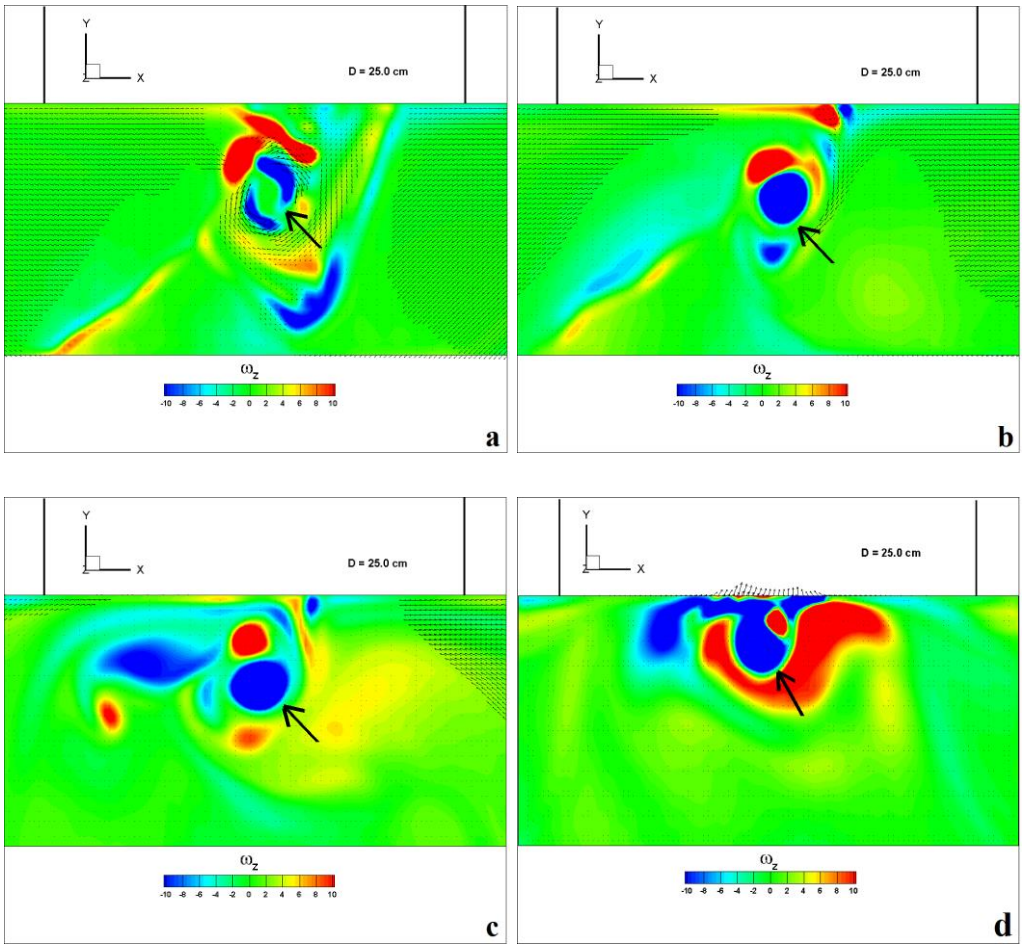

Figure A.22 Case 9: Vertical vorticity contours (ωz, 1/sec) at: a) free water surface; b) just below the visible vortex core; c) mid-S_c level, (h = 42.50 cm); d) top point of intake

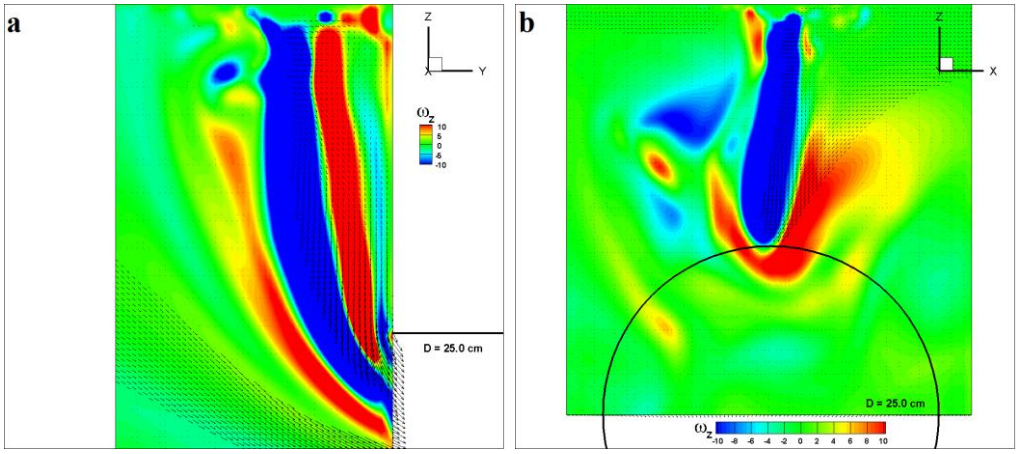

Figure A.23 Case 9: Vorticity contours around z-axis (ω_z, 1/sec): a) longitudinal cross section; b) transverse cross section

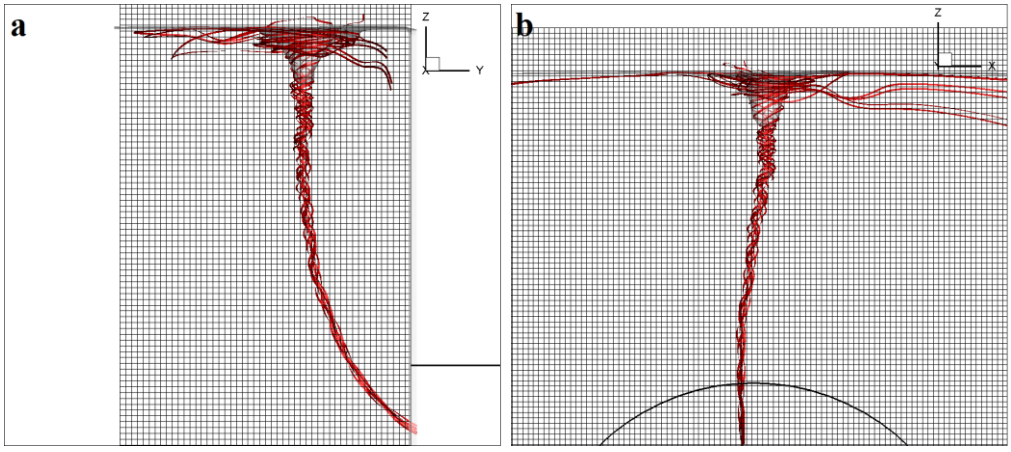

Figure A.24 Case 9: Air-water interface isosurfaces together with the 3D streamlines: a) longitudinal cross section; b) transverse cross section

Case 10: D = 25.00 cm, b_{left} = 50.00 cm, b_{right} = 60.00 cm, Q = 46.75 l/s

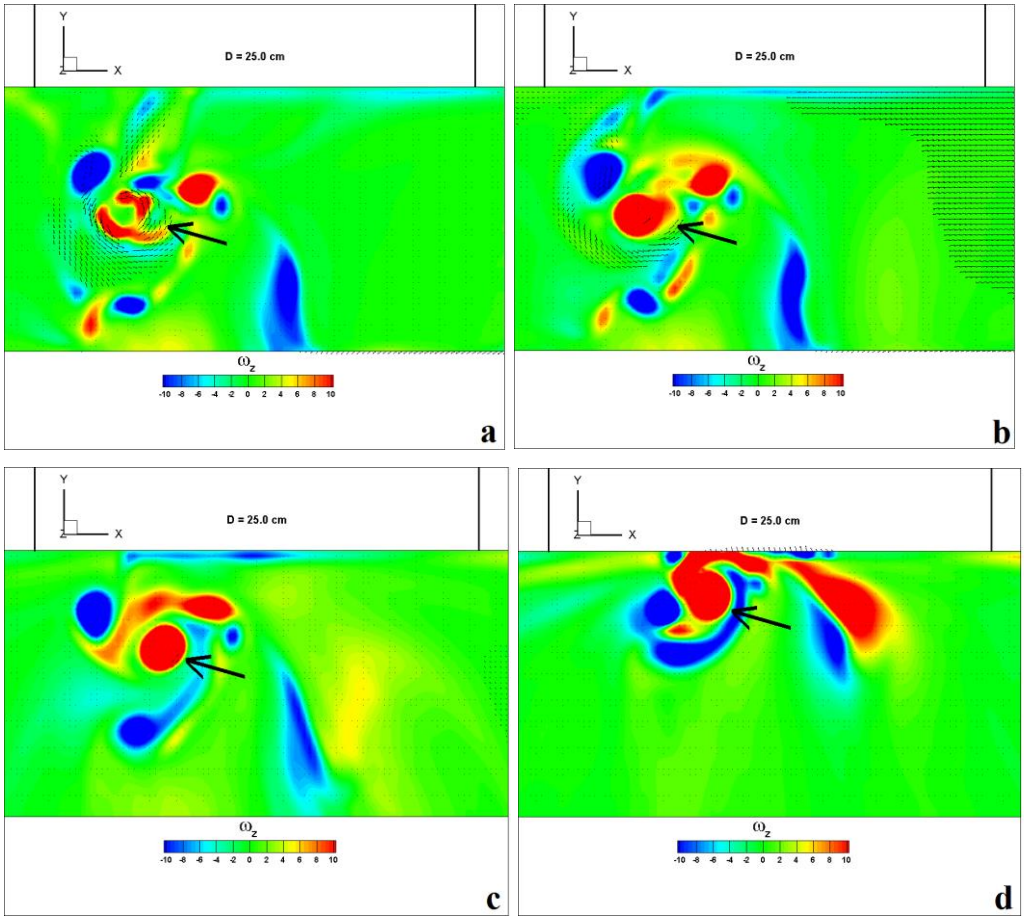

Figure A.25 Case 10: Vertical vorticity contours (ωz, 1/sec) at: a) free water surface; b) just below the visible vortex core; c) mid-S_c level, (h = 40.00 cm); d) top point of intake

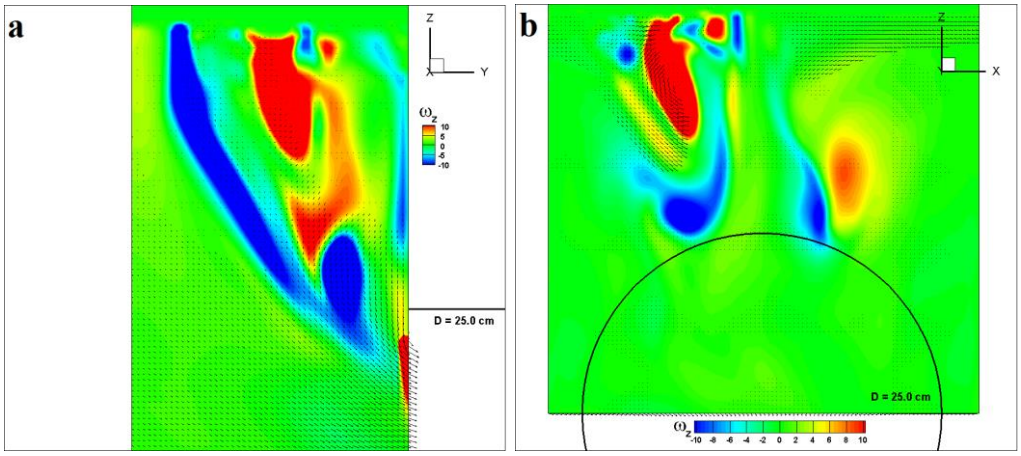

Figure A.26 Case 10: Vorticity contours around z-axis (ωz, 1/sec): a) longitudinal cross section; b) transverse cross section

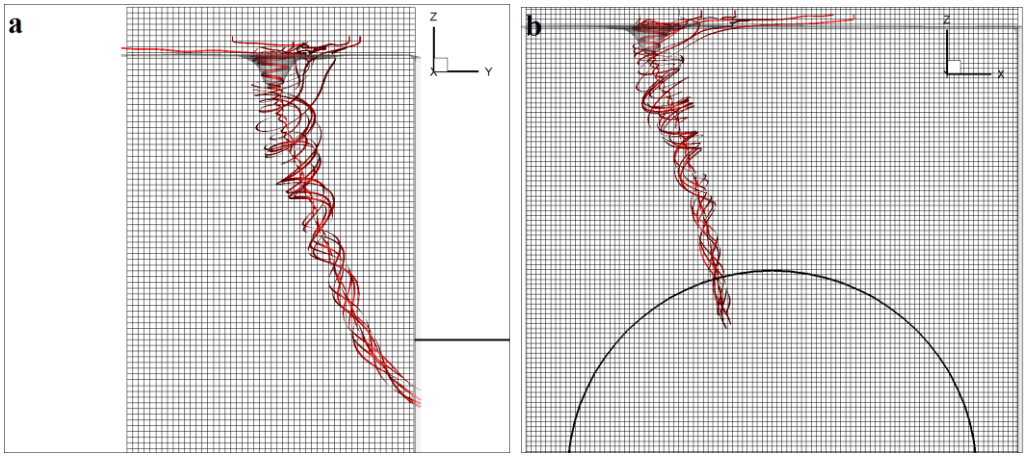

Figure A.27 Case 10: Air-water interface isosurfaces together with the 3D streamlines: a) longitudinal cross section; b) transverse cross section

Case 11: D = 25.00 cm, b_{left} = 50.00 cm, b_{right} = 70.00 cm, Q = 44.18 l/s

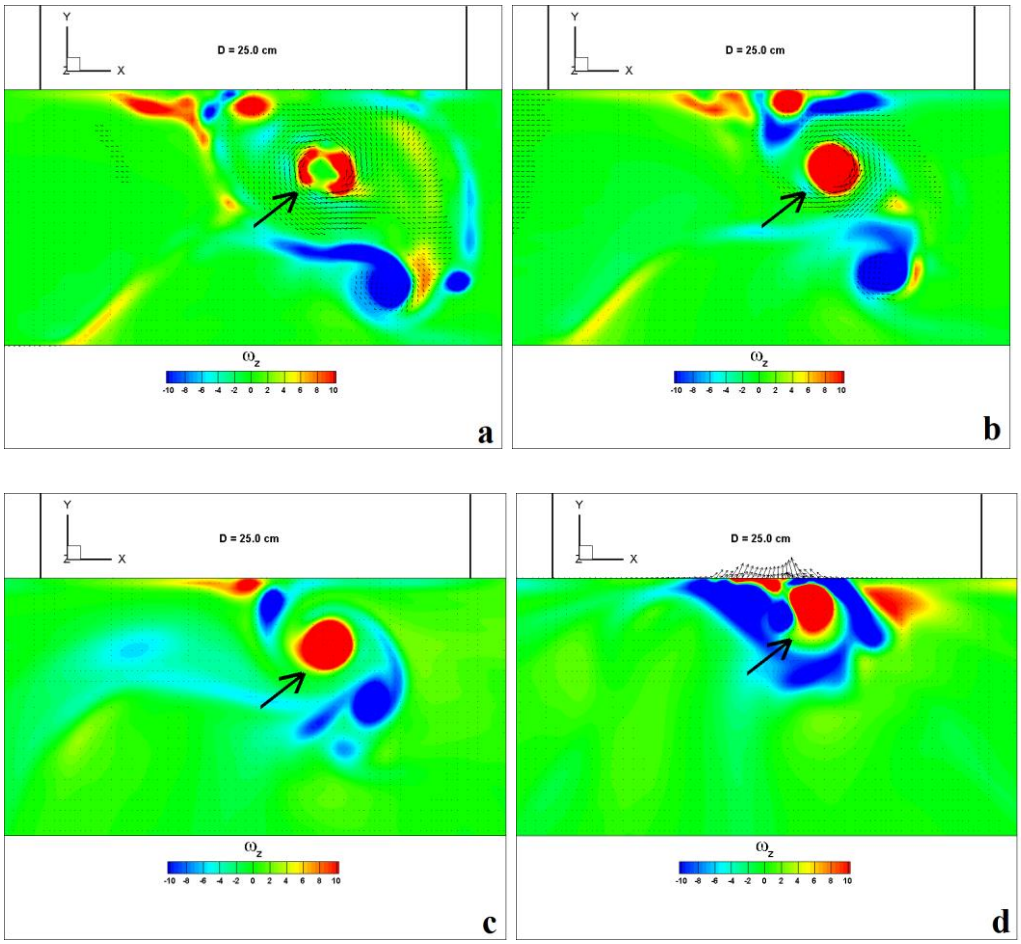

Figure A.28 Case 11: Vertical vorticity contours (ωz, 1/sec) at: a) free water surface; b) just below the visible vortex core; c) mid-S_c level, (h = 42.50 cm); d) top point of intake

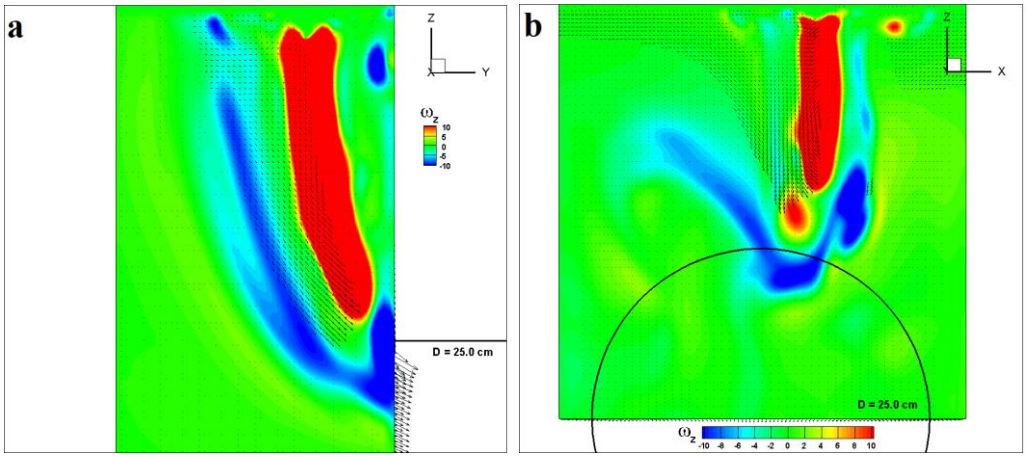

Figure A.29 Case 11: Vorticity contours around z-axis (ωz, 1/sec): a) longitudinal cross section; b) transverse cross section

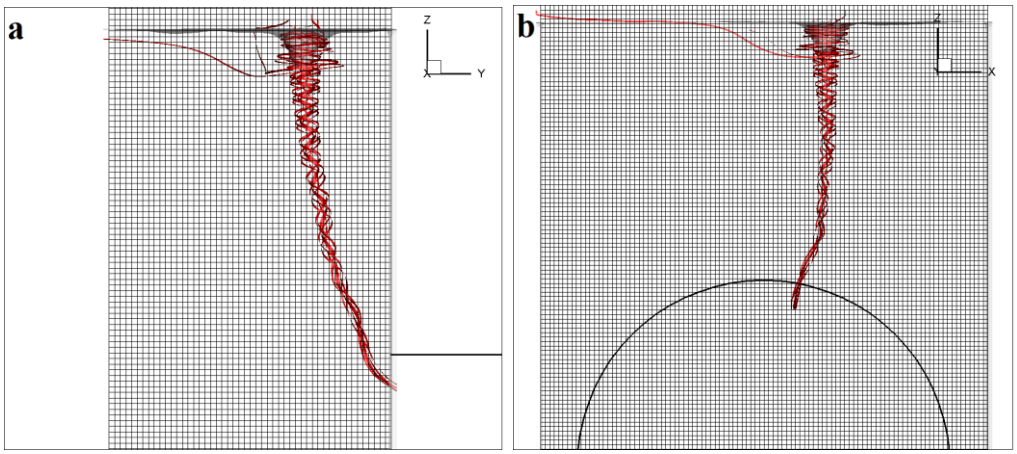

Figure A.30 Case 11: Air-water interface isosurfaces together with the 3D streamlines: a) longitudinal cross section; b) transverse cross section

Case 12: D = 25.00 cm, b_{left} = 60.00 cm, b_{right} = 70.00 cm, Q = 49.38 l/s

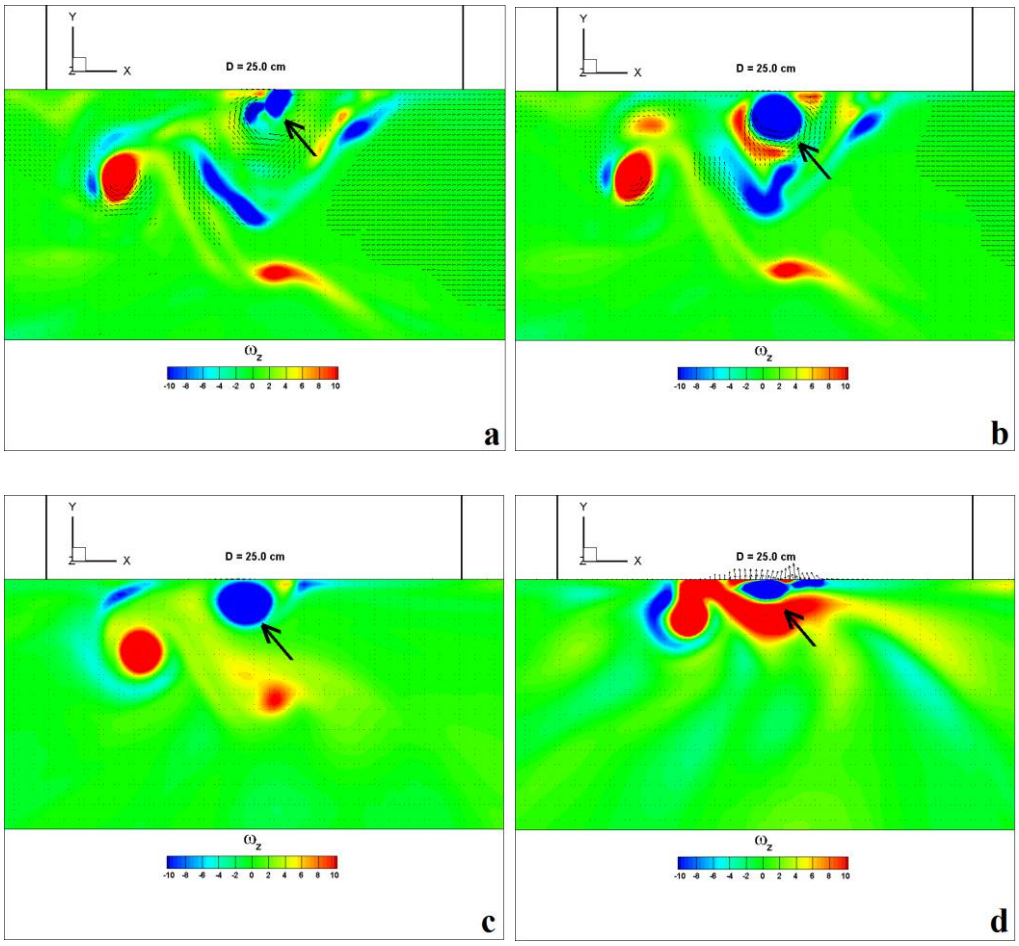

Figure A.31 Case 12: Vertical vorticity contours (ωz, 1/sec) at: a) free water surface; b) just below the visible vortex core; c) mid-S_c level, (h = 42.50 cm); d) top point of intake

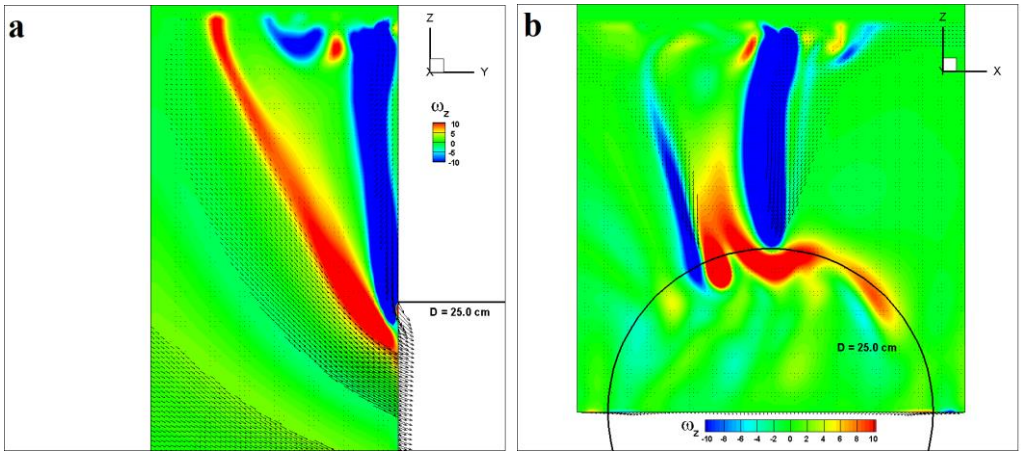

Figure A.32 Case 12: Vorticity contours around z-axis (ωz, 1/sec): a) longitudinal cross section; b) transverse cross section

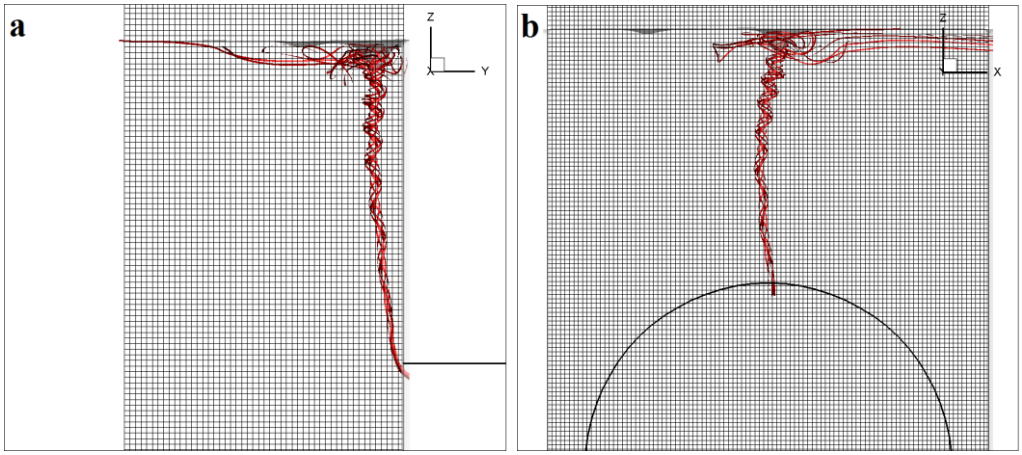

Figure A.33 Case 12: Air-water interface isosurfaces together with the 3D streamlines: a) longitudinal cross section; b) transverse cross section

Case 13: D = 10.00 cm, b_{left} = 20.00 cm, b_{right} = 30.00 cm, Q = 16.64 l/s

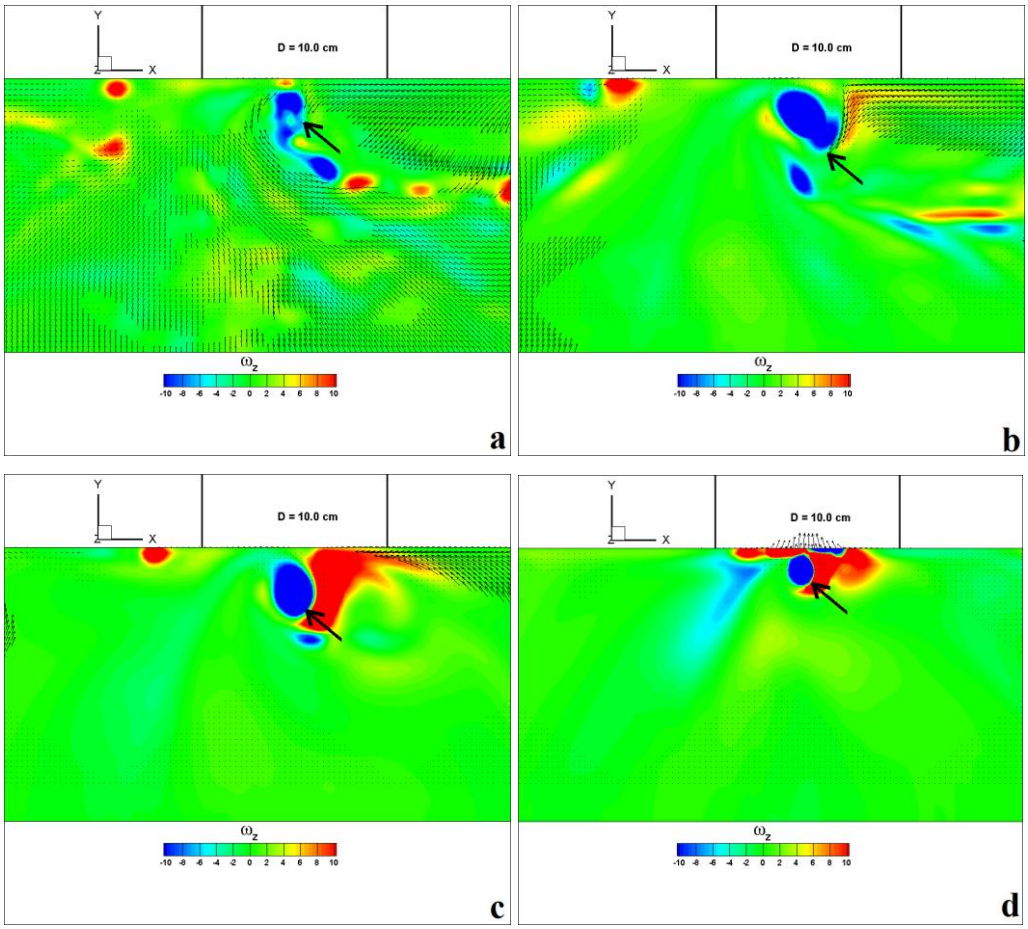

Figure A.34 Case 13: Vertical vorticity contours (ωz, 1/sec) at: a) free water surface; b) just below the visible vortex core; c) mid-S_c level, (h = 22.50 cm); d) top point of intake

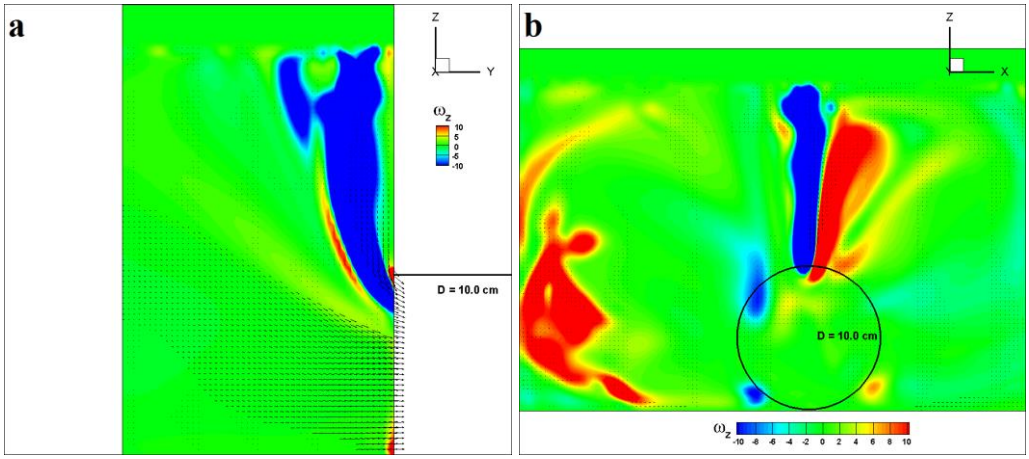

Figure A.35 Case 13: Vorticity contours around z-axis (ωz, 1/sec): a) longitudinal cross section; b) transverse cross section

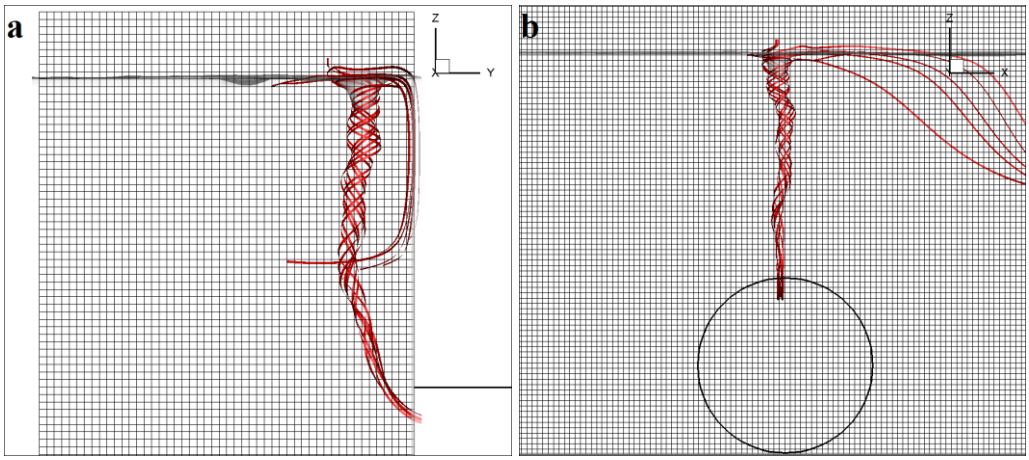

Figure A.36 Case 13: Air-water interface isosurfaces together with the 3D streamlines: a) longitudinal cross section; b) transverse cross section

Case 14: D = 10.00 cm, b_{left} = 20.00 cm, b_{right} = 40.00 cm, Q = 17.23 l/s

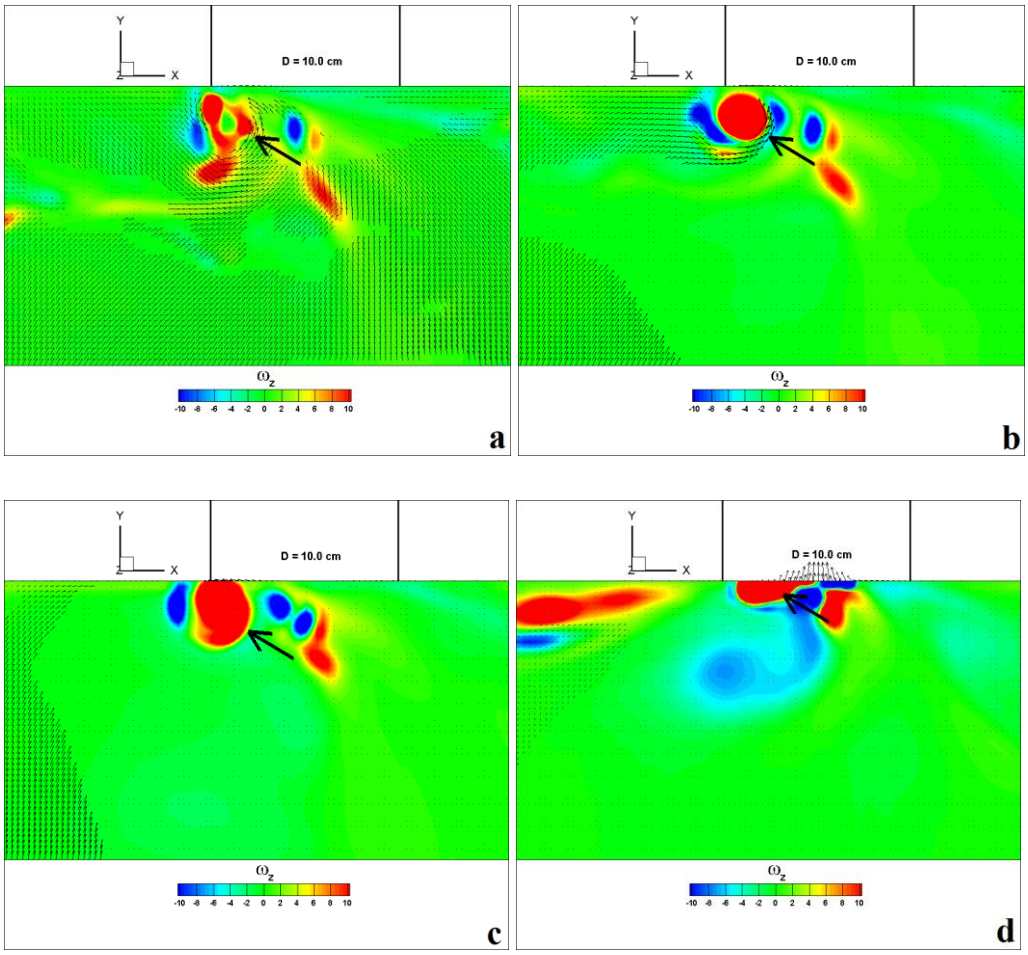

Figure A.37 Case 14: Vertical vorticity contours (ωz, 1/sec) at: a) free water surface; b) just below the visible vortex core; c) mid-S_c level, (h = 22.50 cm); d) top point of intake

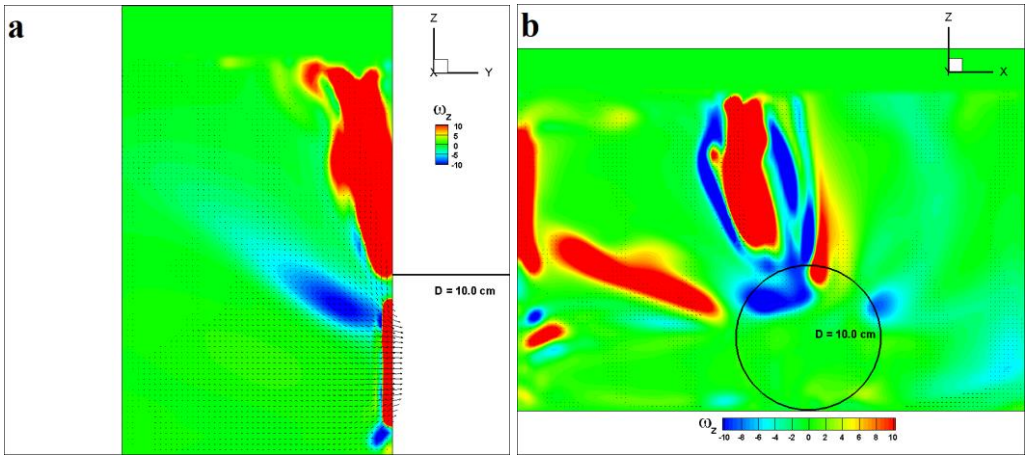

Figure A.38 Case 14: Vorticity contours around z-axis (ωz, 1/sec): a) longitudinal cross section; b) transverse cross section

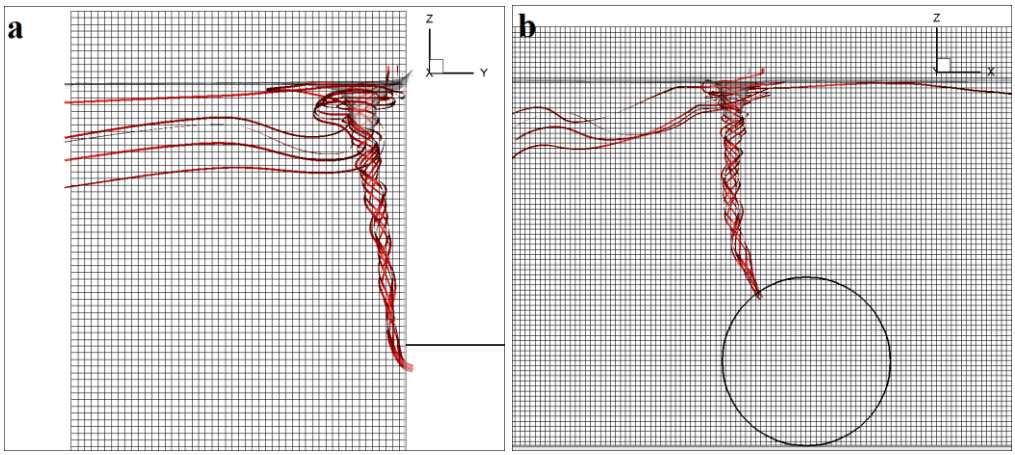

Figure A.39 Case 14: Air-water interface isosurfaces together with the 3D streamlines: a) longitudinal cross section; b) transverse cross section

Case 15: D = 10.00 cm, b_{left} = 20.00 cm, b_{right} = 50.00 cm, Q = 16.64 l/s

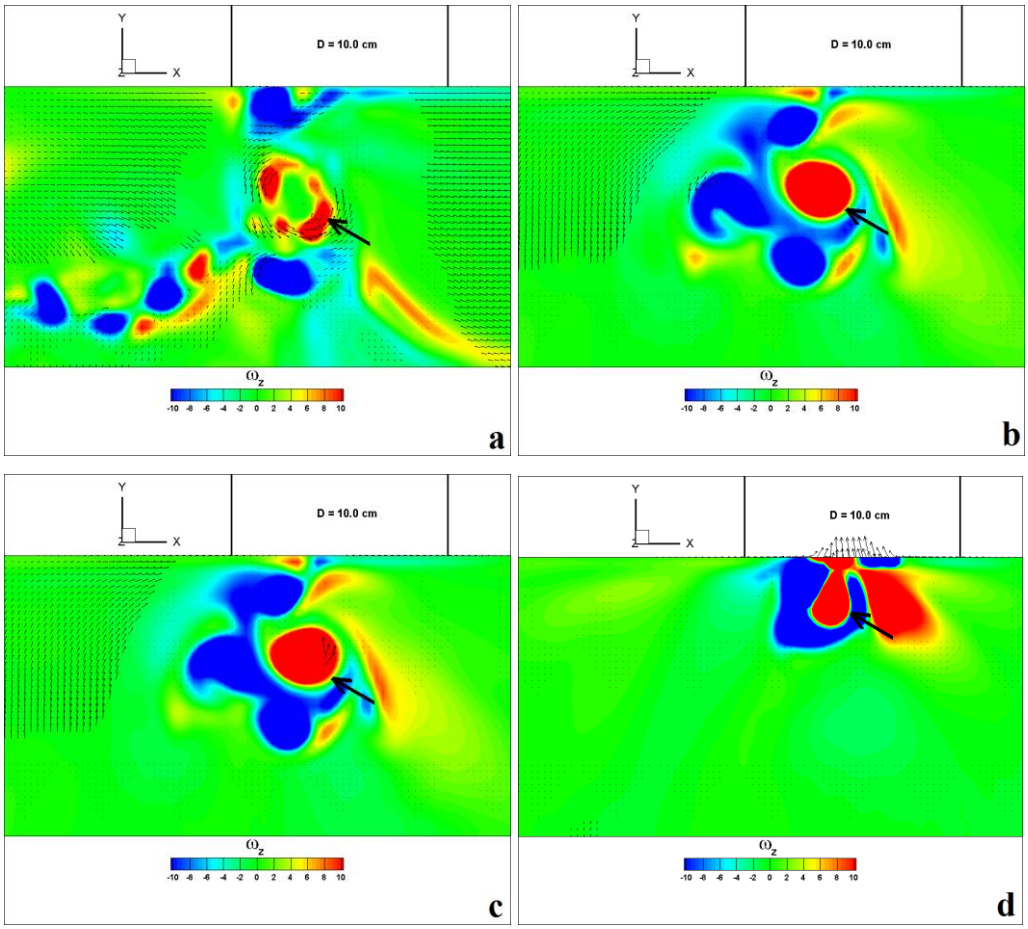

Figure A.40 Case 15: Vertical vorticity contours (ωz, 1/sec) at: a) free water surface; b) just below the visible vortex core; c) mid-S_c level, (h = 20.00 cm); d) top point of intake

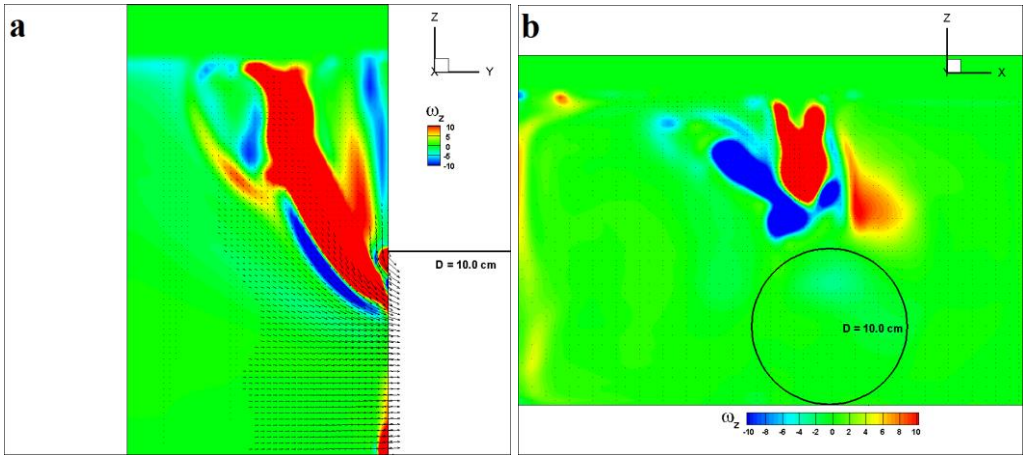

Figure A.41 Case 15: Vorticity contours around z-axis (ωz, 1/sec): a) longitudinal cross section; b) transverse cross section

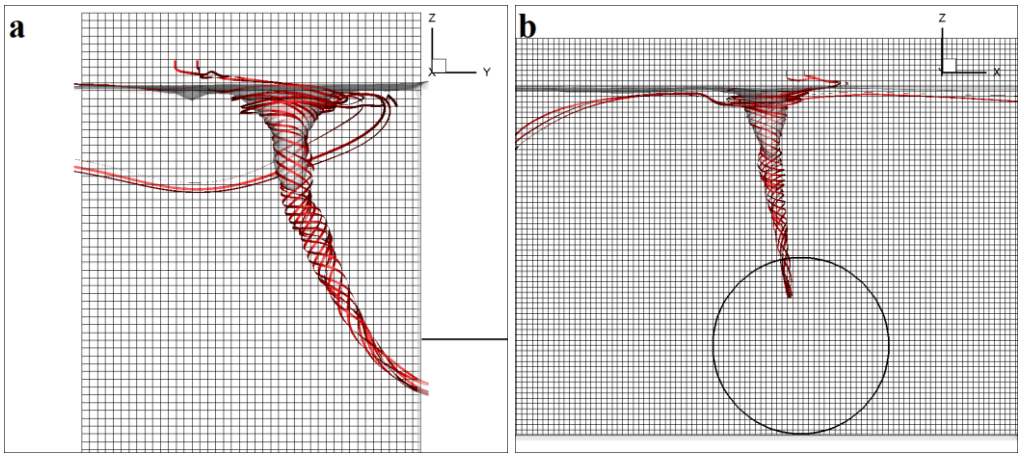

Figure A.42 Case 15: Air-water interface isosurfaces together with the 3D streamlines: a) longitudinal cross section; b) transverse cross section

Case 16: D = 10.00 cm, b_{left} = 30.00 cm, b_{right} = 40.00 cm, Q = 17.84 l/s

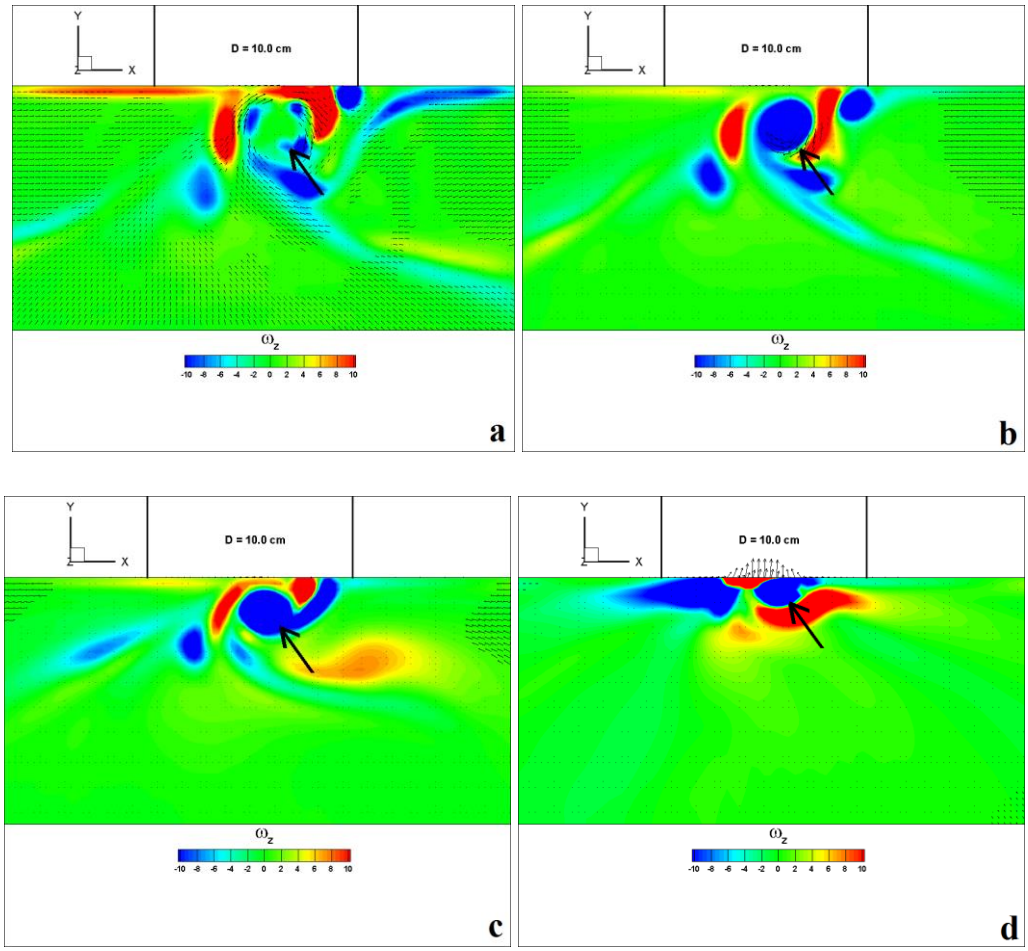

Figure A.43 Case 16: Vertical vorticity contours (ωz, 1/sec) at: a) free water surface; b) just below the visible vortex core; c) mid-S_c level, (h = 22.50 cm); d) top point of intake

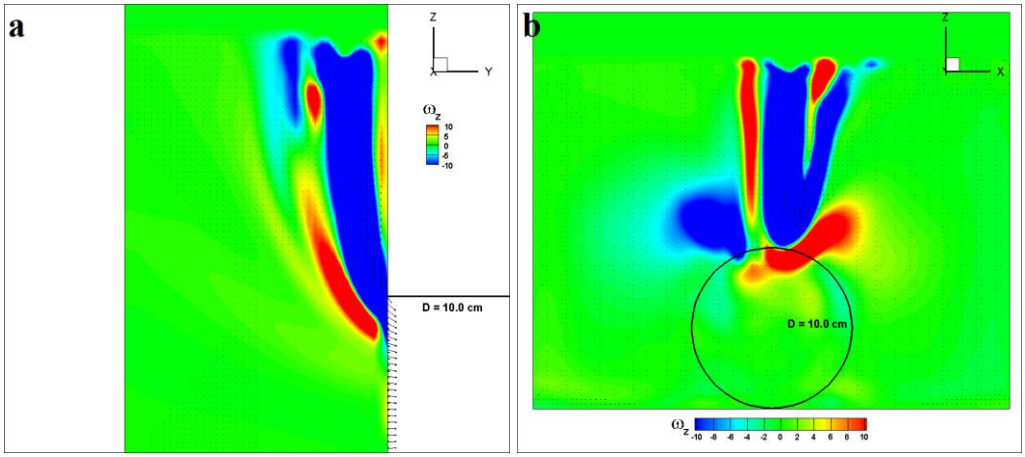

Figure A.44 Case 16: Vorticity contours around z-axis (ωz, 1/sec): a) longitudinal cross section; b) transverse cross section

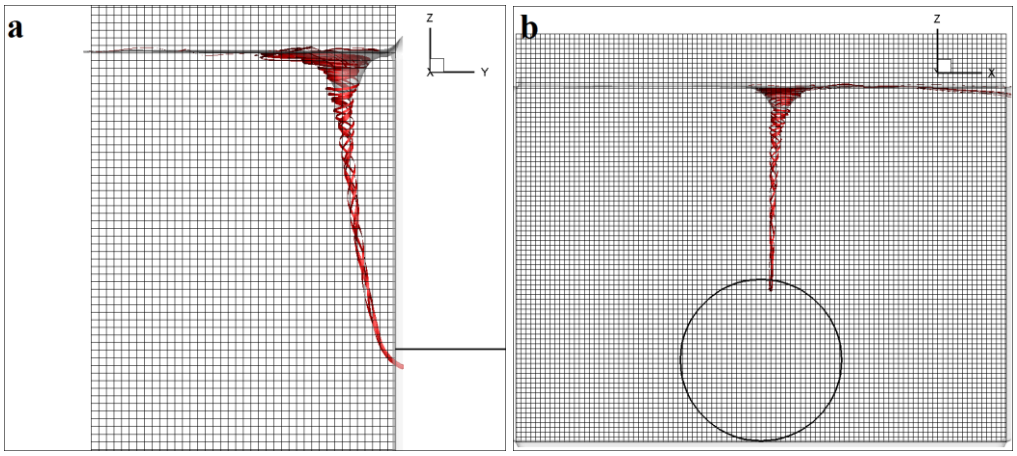

Figure A.45 Case 16: Air-water interface isosurfaces together with the 3D streamlines: a) longitudinal cross section; b) transverse cross section

Case 17: D = 10.00 cm, b_{left} = 30.00 cm, b_{right} = 50.00 cm, Q = 22.92 l/s

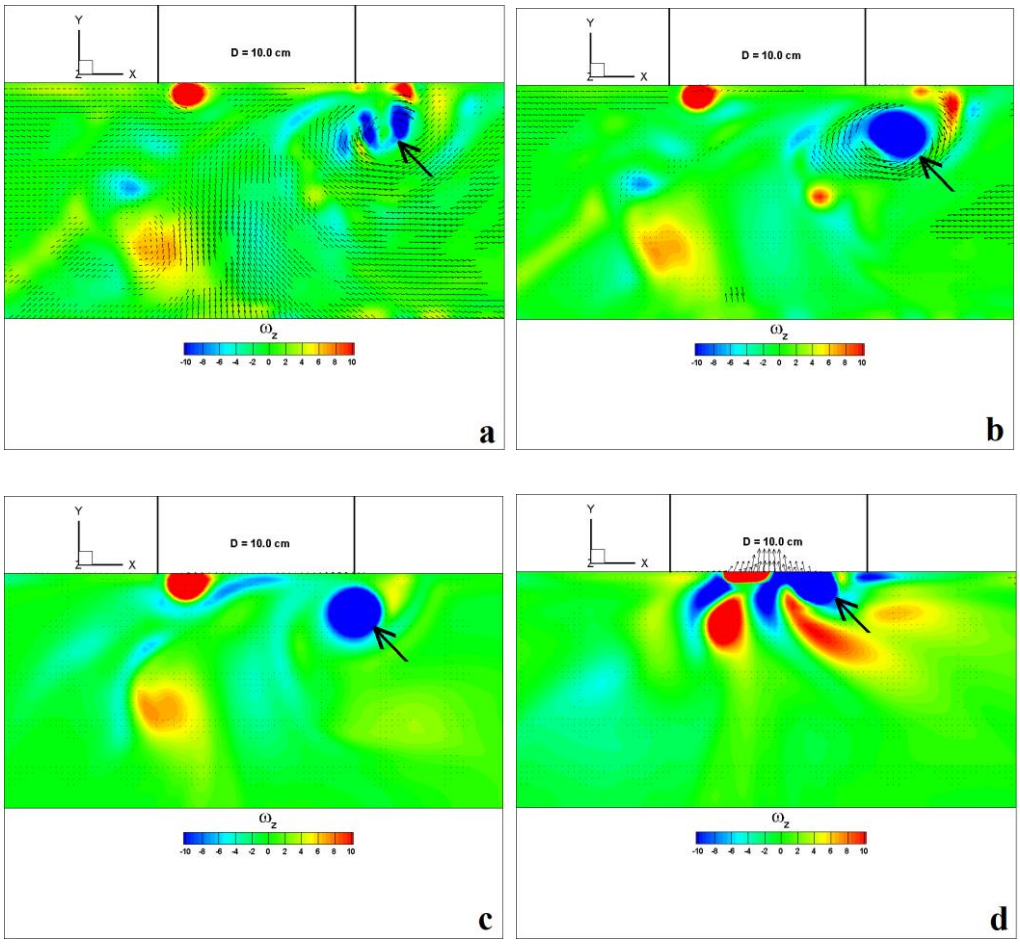

Figure A.46 Case 17: Vertical vorticity contours (ωz, 1/sec) at: a) free water surface; b) just below the visible vortex core; c) mid-S_c level, (h = 30.00 cm); d) top point of intake

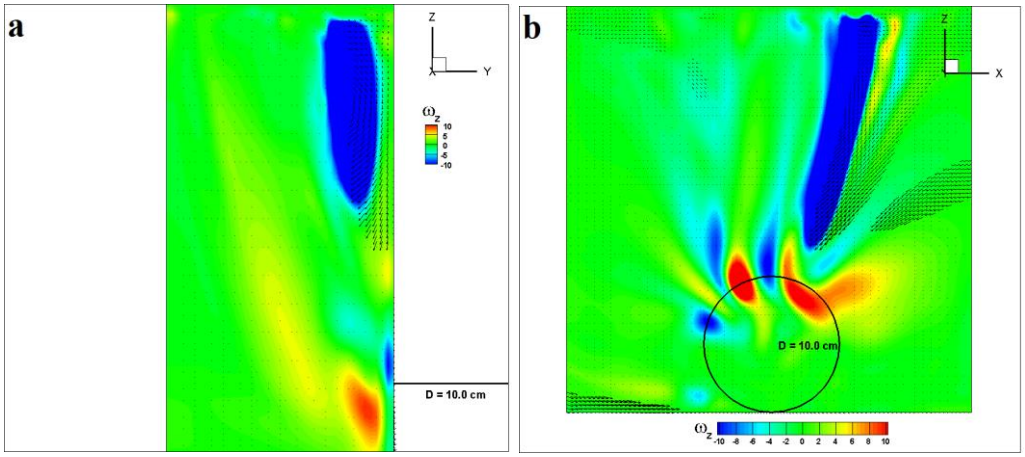

Figure A.47 Case 17: Vorticity contours around z-axis (ωz, 1/sec): a) longitudinal cross section; b) transverse cross section

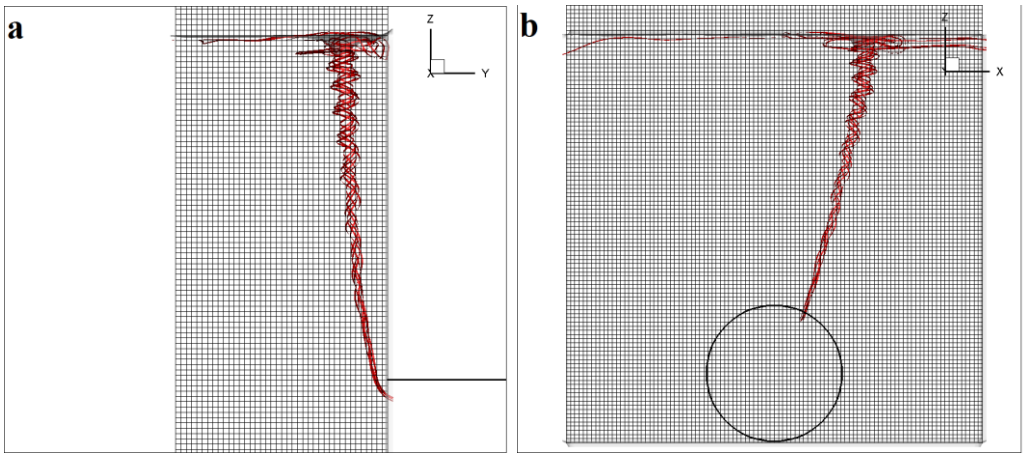

Figure A.48 Case 17: Air-water interface isosurfaces together with the 3D streamlines: a) longitudinal cross section; b) transverse cross section

Case 18: D = 10.00 cm, b_{left} = 40.00 cm, b_{right} = 50.00 cm, Q = 22.92 l/s

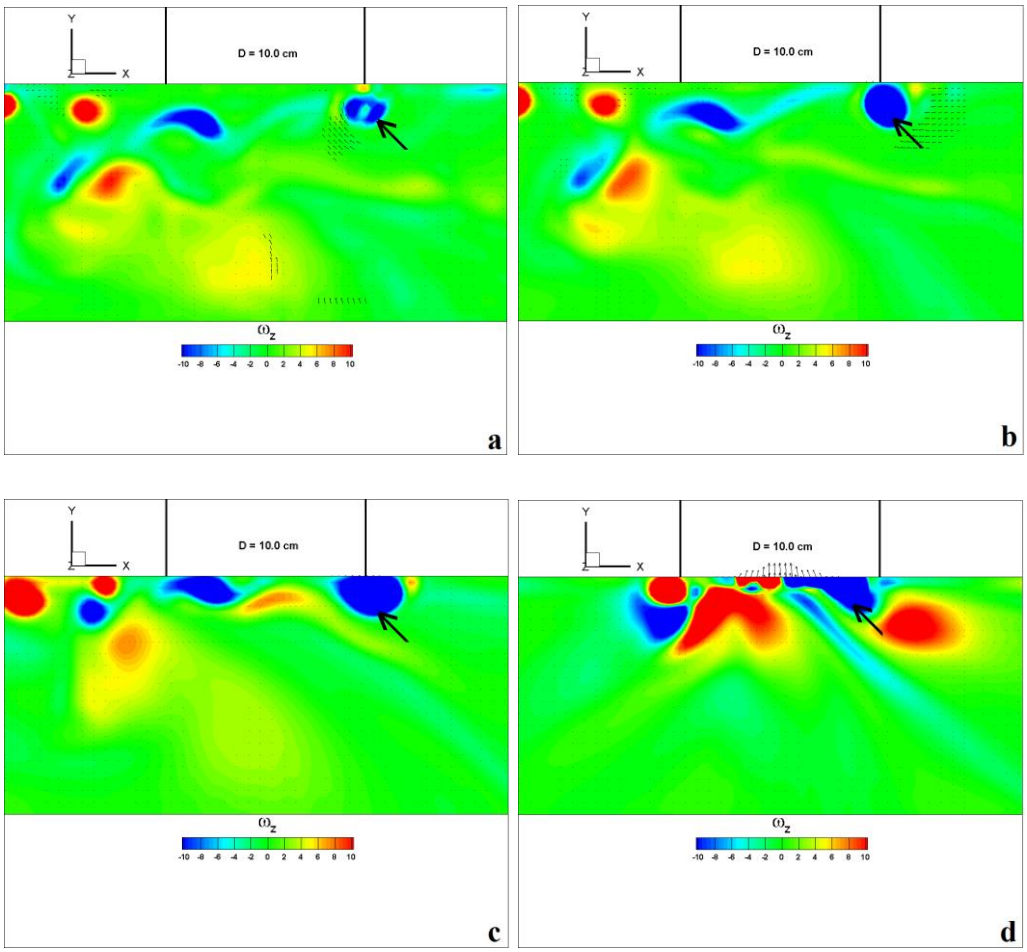

Figure A.49 Case 18: Vertical vorticity contours (ωz, 1/sec) at: a) free water surface; b) just below the visible vortex core; c) mid-S_c level, (h = 30.00 cm); d) top point of intake

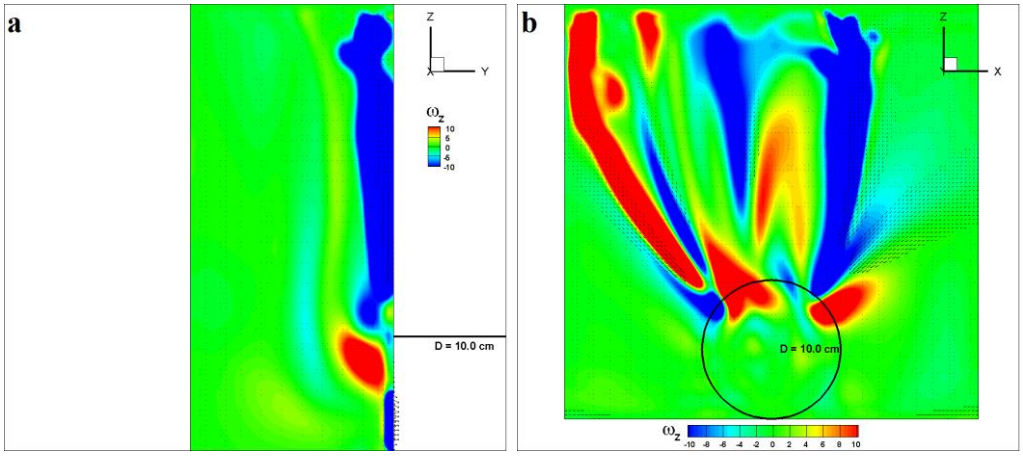

Figure A.50 Case 18: Vorticity contours around z-axis (ωz, 1/sec): a) longitudinal cross section; b) transverse cross section

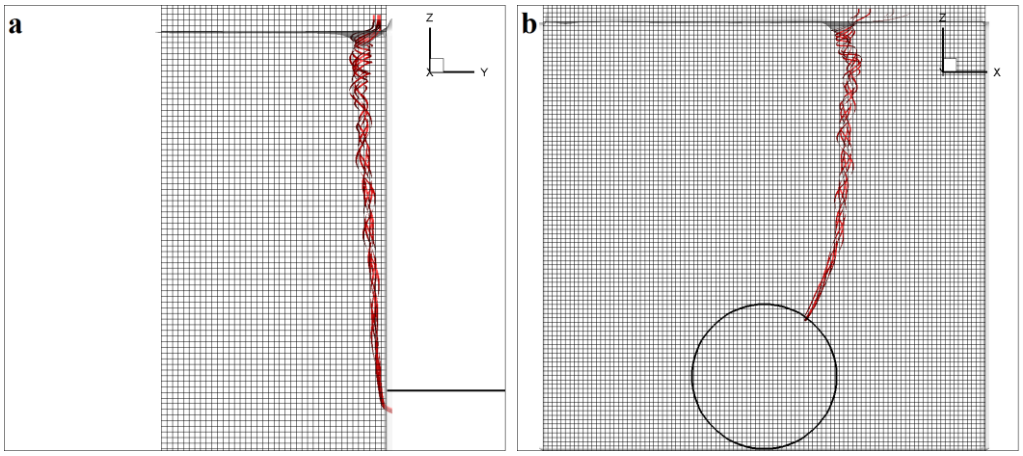

Figure A.51 Case 18: Air-water interface isosurfaces together with the 3D streamlines: a) longitudinal cross section; b) transverse cross section

Case 19: D = 10.00 cm, b_{left} = 50.00 cm, b_{right} = 60.00 cm, Q = 28.47 l/s

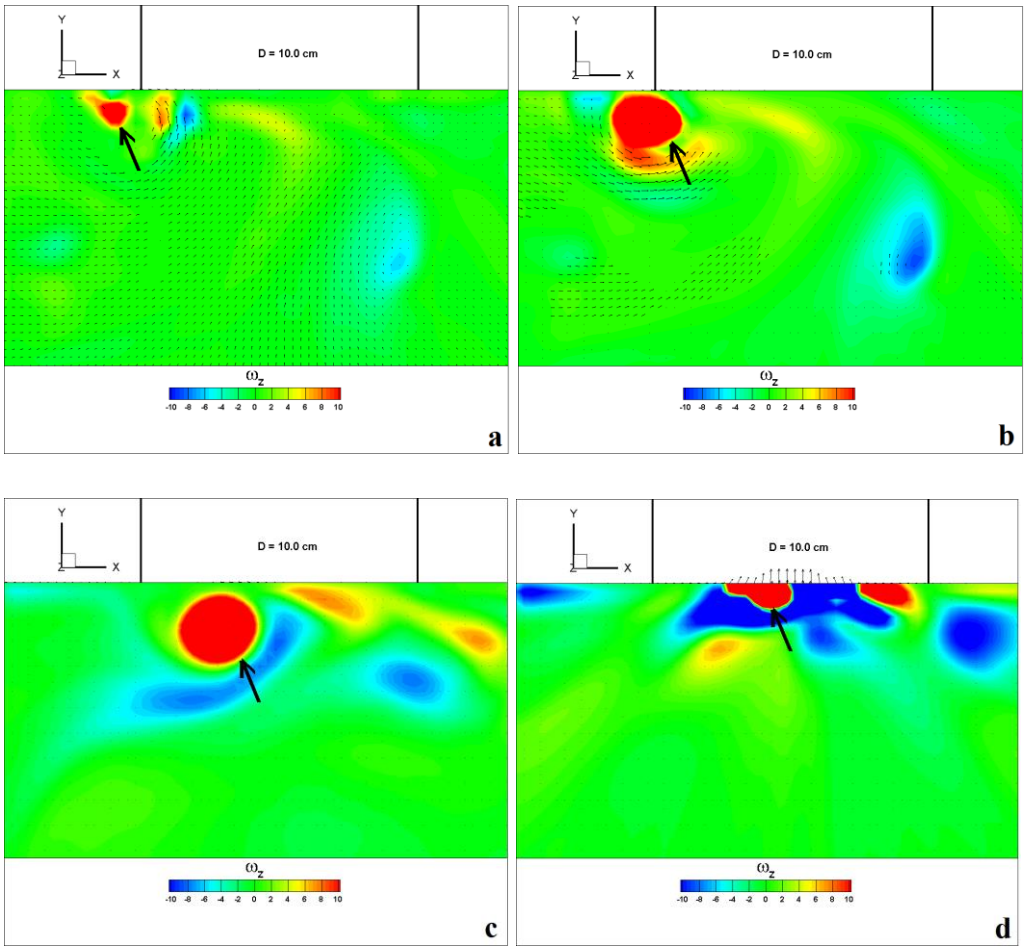

Figure A.52 Case 19: Vertical vorticity contours (ωz, 1/sec) at: a) free water surface; b) just below the visible vortex core; c) mid-S_c level, (h = 32.50 cm); d) top point of intake

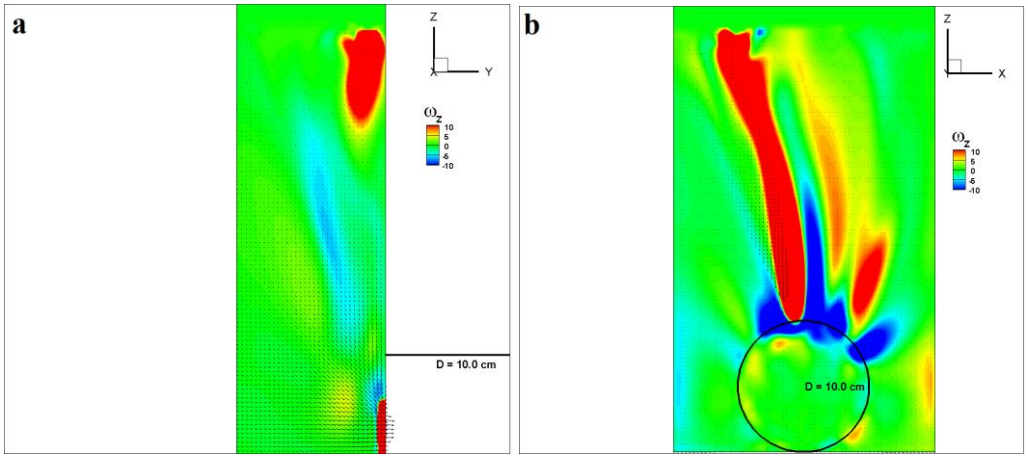

Figure A.53 Case 19: Vorticity contours around z-axis (ωz, 1/sec): a) longitudinal cross section; b) transverse cross section

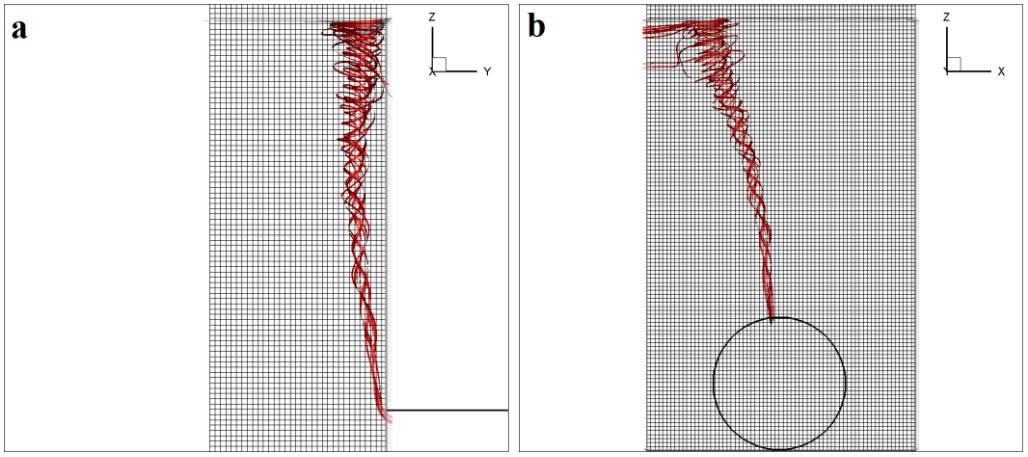

Figure A.54 Case 19: Air-water interface isosurfaces together with the 3D streamlines: a) longitudinal cross section; b) transverse cross section